Advances in Electrocatalytic Semi-hydrogenation of Acetylene in Aqueous Electrolyte:

Progress, Challenges, and Opportunities

Zihao Yan, Libang Xu, and Huiyuan Zhu*

Department of Chemistry, University of Virginia, 409 McCormick Rd, Charlottesville, VA 22904

*Corresponding Author(s): kkx8js@virginia.edu

Abstract

Catalytic hydrogenation is a foundational pillar of the chemical industry. Especially, semi-hydrogenation of

acetylene (C₂H₂) to ethylene (C₂H₄) is an important industrial reaction to generate polymer-grade C₂H₄ from

crude streams for polyethylene production. The industrial C2H2 semi-hydrogenation process is currently

dominated by the thermocatalytic route which involves cost-prohibitive Pd-based catalysts, high operation

temperature, and excess hydrogen feed. Thermocatalytic semi-hydrogenation of C2H2 is also hindered by

limited C₂H₄ selectivity due to unwanted over-hydrogenation. Therefore, seeking strategies to improve the

catalyst performance while reducing energy consumption and capital expenditure of the current hydrogenation

schemes is essential to the petrochemical industry. Fortunately, recent advances in electrocatalytic C₂H₂ semi-

hydrogenation systems lead to a sustainable alternative to traditional thermocatalytic systems. Using

renewable electricity as an energy source and water as a hydrogen source, electrocatalytic systems can operate

under ambient conditions with tunable selectivity toward C₂H₄. In this review, we first discuss the reactor design

for electrocatalytic C₂H₂ semi-hydrogenation. We then review the computational studies for understanding and

predicting the catalytic behavior of metal catalysts. We also summarize advanced electrocatalysts categorized

into Cu-based and non-Cu-based materials. Finally, we provide perspectives on the opportunities to overcome

existing challenges for future practical application of electrocatalytic C_2H_2 semi-hydrogenation.

1

Keywords

Acetylene, Ethylene, Electrocatalysis, Semi-hydrogenation

Introduction

Semi-hydrogenation of Acetylene and Background To meet the growing demand for polymers, ethylene (C₂H₄) as the essential feedstock for polyethylene, is produced over 170 metric tons annually via the cracking of petroleum hydrocarbons, such as naphthas or saturated C2 to C6 hydrocarbons. ^{1, 2} Unfortunately, the produced C₂H₄ stream inevitably contains a trace amount of acetylene (C₂H₂), which poisons the downstream Ziegler-Natta polymerization catalysts. Consequently, the C_2H_2 in the C_2H_4 stream should be reduced to less than 5 ppm to achieve polymer-grade polyethylene.^{3, 4} Industrially, thermocatalytic C₂H₂ semi-hydrogenation using Pdbased catalysts, such as the Lindlar catalyst (Pd supported on CaCO₃ and then treated by lead, Pb)⁵ and PdAg catalysts, 6, 7 has been employed for C₂H₂ removal. 8, 9 However, thermocatalytic semi-hydrogenation of C₂H₂ usually suffers from several drawbacks severely limiting its efficiency and sustainability. Due to the sluggish reaction kinetics, precious metal (mostly Pd)-based catalysts, excess hydrogen (H2) feed, high operation temperature (100-250 °C), and high pressure (5 bar) are required during the C₂H₂ hydrogenation, ^{10, 11} leading to high capital and energy expenditures. In fact, the purification of C2H4 and propene streams accounts for 0.3% of global energy consumption. 12, 13 Another issue is the limited selectivity of Pd-based catalysts. Pd strongly adsorbs C₂H₂ and readily activates H₂ into hydrides.^{6, 14, 15} However, this strong C₂H₂ adsorption and abundance of Pd-hydrides inevitably lead to the over-hydrogenation toward ethane (C₂H₆).⁶, ¹⁶ Moreover, the oligomerization on the catalyst surface leads to the formation of C₄+ products, known as green oil, which deactivates catalysts by blocking their surface active sites. 17, 18 In addition, thermocatalytic routes require an extensive supply of H₂. The industrial production of H₂ heavily relies on steam methane reforming in large central plants, 19, 20 generating 7-11 kg of CO₂ per 1 kg of H₂ generated 21-23. Also, operating with excess H₂ at elevated temperatures not only introduces additional separation costs but also causes safety issues, such as thermal runaway.^{24, 25}

Recent efforts in developing advanced thermocatalysts with improved performance can be categorized into two main strategies. One strategy is to tune and optimize the adsorption of C_2H_x species through catalyst design, such as constructing single-atom catalysts (SACs) whose isolated Pd sites exhibit mild π -mode adsorption of C_2H_x and alloying Pd with a second metal to weaken the adsorption of C_2H_x . The other strategy is to inhibit the formation of energetic subsurface Pd hydrides by establishing core-shell and yolk-shell structures. Thermocatalytic acetylene semi-hydrogenation has been extensively reviewed elsewhere. Nevertheless, these strategies lead to a trade-off between activity and selectivity due to the scaling relationship among C_2H_x species or limited mass transport. Consequently, simultaneously achieving high C_2H_2 conversion (>90 %) and high C_2H_4 selectivity (>90%) under mild conditions (< 100 °C) remains challenging. Therefore, searching for high-performing, green alternatives with smaller infrastructure to the thermocatalytic systems is urgent to produce polymer-grade C_2H_4 feeds.

Electrocatalytic Semi-hydrogenation of Acetylene and Overview The recent surge in renewable energy growth calls for a paradigm shift in decentralized, and sustainable chemical conversions that can be powered by renewable electricity from solar and wind. Compared with the conventional energy-and CO₂-intensive thermocatalytic routes, electrocatalytic systems allow distributed operations under ambient conditions (room temperature and atmospheric pressure) with a green hydrogen source either directly from water or the water-splitting reaction.^{34, 35} In recent years, extensive progress in electrocatalysis has been made rapidly covering many important reactions such as hydrogen evolution reaction (HER), ³⁶⁻³⁸ CO₂ reduction reaction (CO₂RR), ³⁹⁻⁴¹ and ammonia synthesis.⁴²⁻⁴⁴ In the case of electrocatalytic semi-hydrogenation of C₂H₂ in aqueous electrolytes, water instead of H₂ directly serves as the hydrogen source. The overall reaction is Equation 1:

$$C_2H_2 + 2H_2O + 2e^- \rightarrow C_2H_4 + 2OH^-, E^0 = 0.733 V \text{ vs. RHE.}^{45}$$
 (1)

In situ generation and consumption of the active hydrogen source from water not only avoids the excess feed of H_2 , preventing the over-hydrogenation toward C_2H_6 but also enhances the safety and economy of the system.

In addition, developing electrocatalysts for C₂H₂ reduction can potentially go beyond high-cost precious metals because earth-abundant metals such as Ni,^{46, 47} Fe,^{48, 49} and Cu^{41, 50} have been widely used in electrocatalytic reactions. In fact, fascinating progress has been made recently in employing non-precious metals in electrocatalytic C₂H₂ semi-hydrogenation, which will be the focus of our review. Research into electrocatalytic C₂H₂ semi-hydrogenation can be traced back to the 1960s when Burke et al. demonstrated the hydrogenation of C₂H₂ on Pd and Pt electrodes.⁵¹ Since then, metal electrocatalysts including Pt,^{52,53} Pd,⁵⁴ Cu⁵⁴, and Ag⁵⁵ have been investigated, which, however, suffer from limited current density, C₂H₄ selectivity, and Faradaic efficiency (FE). Two obstacles that plagued the catalytic performance in these early studies are the poor solubility of C₂H₂ in water (1200 mg/L at 25 °C)⁵⁶ and the competition of side reactions such as C-C coupling into 1,3-butadiene and HER; the latter is a common competing reaction for many electrochemical reduction reactions, e.g. CO₂RR.⁵⁷⁻⁵⁹

To achieve sufficient coverage of C_2H_2 on the electrocatalyst surface for suppressing the HER and to improve the space velocity (SV) for economic viability, the solubility issue must be addressed before the widespread application of the electrocatalytic C_2H_2 semi-hydrogenation systems. In addition, unlike other electrocatalytic reactions, such as CO_2RR which feeds in pure reactants, only $\leq 1\%$ C_2H_2 exists in the feed stream for the semi-hydrogenation reaction to simulate industrial crude streams, adding one additional barrier to solve the solubility issue. One potential solution is to apply an organic solvent for C_2H_2 such as N, N-dimethylformamide as the electrolyte. This method, nevertheless, is limited by an insufficient proton source and the high cost associated with organic solvents. Fortunately, the rapid advancement of gas diffusion layers (GDL), has enabled direct and prolonged contact of gas-phase reactants with electrocatalysts in aqueous electrolytes through a gas/electrolyte/catalyst interface. Recent studies of GDL-based flow cells demonstrate that they can successfully overcome the mass-transport limitations by continuously circulating the reactants and products to and away from the electrodes. The computational insights are also of paramount importance because these studies decipher the reaction mechanism and the nature of catalyst-adsorbate interactions, facilitating catalyst screening and selection. These recent advancements in GDL-based reactors and computational insights have

enabled the rational design of electrocatalysts to maximize the C_2H_2 conversion and C_2H_4 selectivity. In this review, we summarize the recent progress in electrocatalytic C_2H_2 semi-hydrogenation, discussing reactor architectures, computational insights, and electrocatalyst design as illustrated in **Fig. 1**. We also provide indepth discussions of the challenges in the field and potential strategies to develop more advanced electrocatalytic C_2H_2 semi-hydrogenation systems.

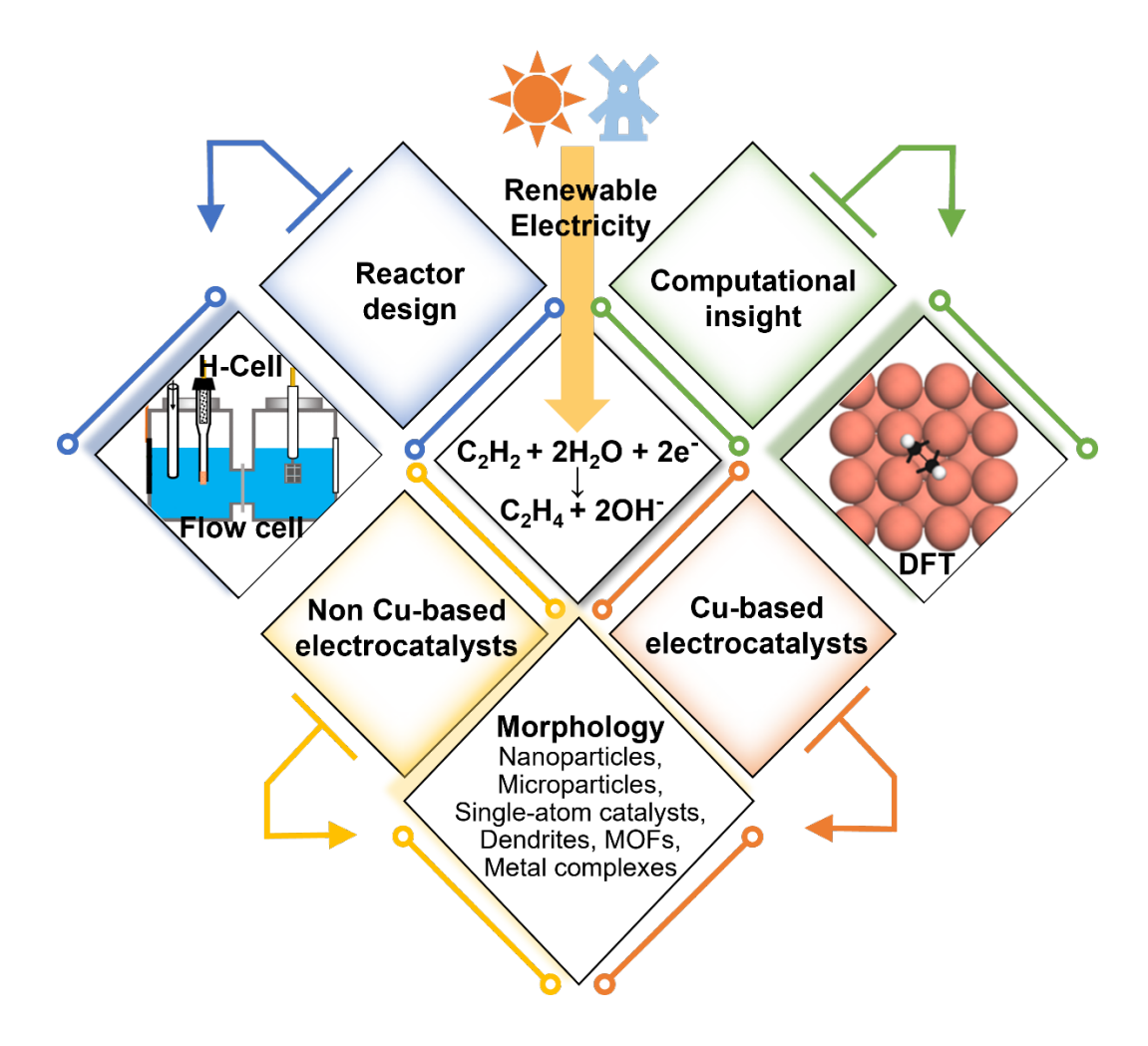


Fig. 1. Schematic overview of the topics covered in this review.

Electrocatalytic Semi-hydrogenation of Acetylene: Reactor Architectures, Computational Insights, and Electrocatalysts

Reactor Architectures H-cell is the most widely used reactor for many electrocatalytic reactions due to operational simplicity, high adaptability, and low cost. As shown in Fig. 2a, a typical H-cell with a three-electrode system contains an anode chamber and a cathode chamber separated by an ion-exchange membrane. The separation of anode and cathode chambers minimizes the interference from reactions at the counter electrode and facilitates product separation and collection. The results obtained from H-cells can often be interpreted to understand the reactivity trend and structure-property relationships of the electrocatalytic systems.

The performance of electrocatalytic systems in H-cells is hampered by limited current densities (< 100 mA/cm²) that do not resemble the dynamic environment of commercially viable electrolyzes. ^{59, 64} To overcome the mass transport limitations, especially when a gaseous reactant with limited solubility is involved, flow cells equipped with GDL-coated carbon paper (GDL-CP) are more frequently employed for electrocatalytic C₂H₂ semi-hydrogenation in recent years. GDL is a typically multi-layered carbon-based porous material with balanced hydrophobicity and hydrophilicity, containing a macro-porous/micro-porous substrate or backing (**Fig. 2b**). Compared with the pristine carbon paper that is commonly used in the H-cell setup, GDL-CP has an inherently high surface area and porosity, promoting the mass transfer and local concentration of C₂H₂. Flow cells can further overcome the diffusion limit in the liquid phase by continuously flowing electrolytes over catalysts. Moreover, inspired by the success of membrane electrode assembly (MEA) electrodes designed for low-temperature fuel cells and water electrolyzers, ^{65, 66} flow cells used nowadays are mostly membrane-based due to their selective transportation of ions such as protons and hydroxides. One early study of electrocatalytic hydrogenation of C₂H₂ in an electrochemical membrane reactor demonstrates that electrochemically generated hydrogen reacted with C₂H₂ during semi-hydrogenation on a Cu cathode. ⁵⁴ A typical design of a 3-electrode membrane-based flow cell contains an anode chamber for the water oxidation, a cathode chamber for C₂H₂

hydrogenation, and a gaseous chamber for the feed of reactant (Fig. 2c). The anode and cathode chambers are separated by an ion exchange membrane such as a proton exchange membrane (PEM) or an anion exchange membrane (AEM). The electrolyte (typically 1 M KOH) is refluxed to the anode and cathode chamber by a peristaltic pump. The cathode chamber and gaseous chamber are separated by carbon paper with a highly porous GDL, which also serves as the working electrode. Electrocatalysts are coated on one side of the carbon paper, which is directly in contact with the electrolyte, while the hydrophobic side of the GDL prevents the aqueous electrolyte from entering the gas chamber. A Hg/HgO electrode and nickel foam are commonly used as the reference and counter electrode respectively. During the reaction, the gaseous reactant readily diffuses through the GDL and directly interacts with the electrocatalyst layer in the cathode chamber as illustrated in Fig. 2b. In the meanwhile, continuous electrolyte/reactant circulation by the peristaltic pumping ensures sufficient convective mass transfer of reactant gas into the cathode chamber.

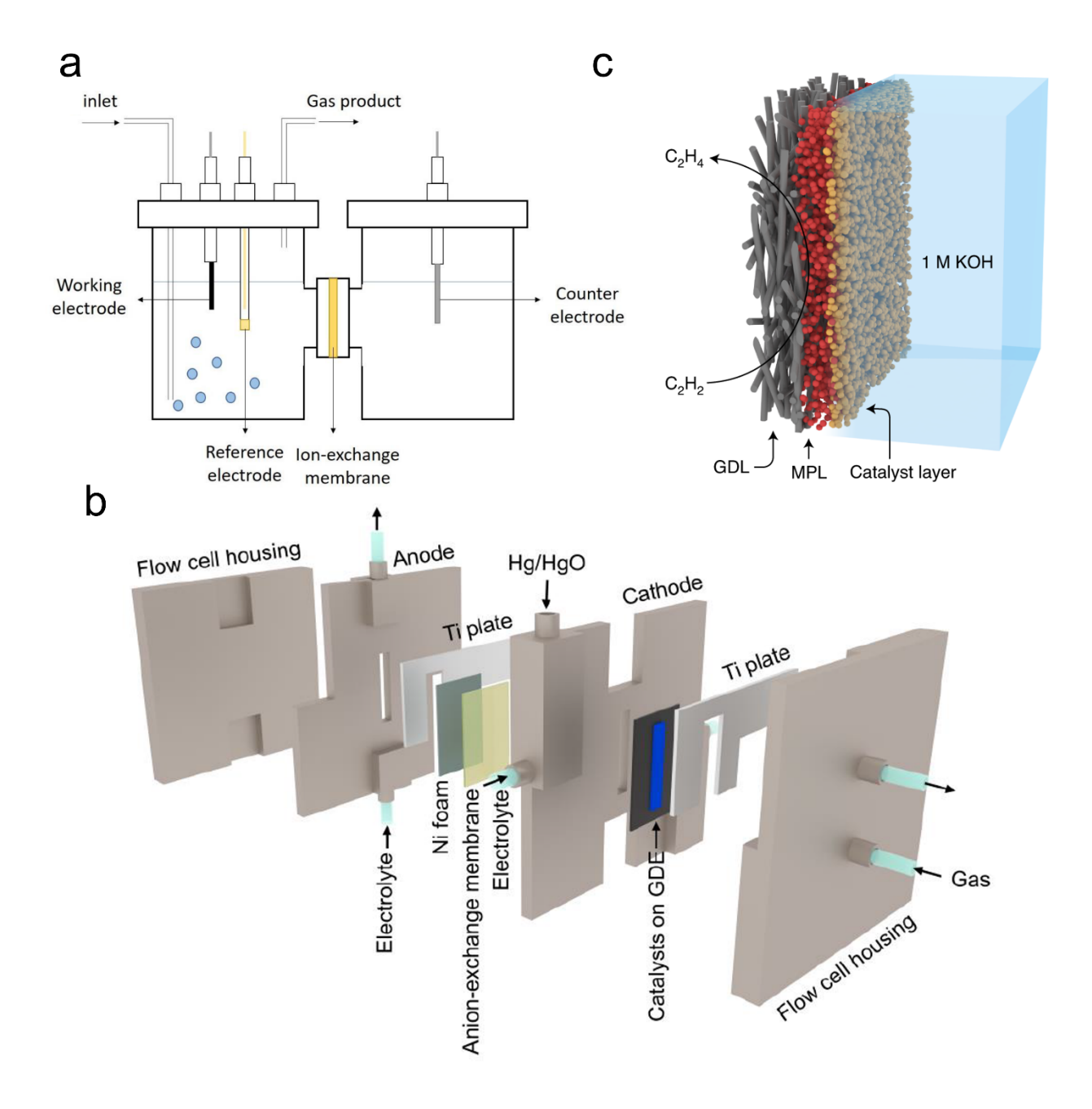


Fig. 2. a) Schematic illustration of a 3-electrode H-cell. Reproduced with permission.⁶³ Copyright 2020, MDPI. b) Schematic illustration of the cathode and gaseous chamber of a flow cell used for electrocatalytic C₂H₂ semi-hydrogenation (MPL: microporous layer). Reproduced with permission.⁶⁷ Copyright 2021, Nature Publishing Group. c) Schematic illustration of a 3-electrode flow cell. Reproduced with permission.⁶⁸ Copyright 2022, Chinese Chemical Society.

Reaction Mechanisms and Computational Insights The electrocatalytic hydrogenation of C_2H_2 has been proposed to follow a series of proton-electron coupling steps as illustrated in Fig. 3a. The reaction begins with the adsorption of C_2H_2 and its protonation into *CHCH₂ coupled with electron transfer. The semi-hydrogenation pathway (blue arrows) and the over-hydrogenation pathway (red arrows) bifurcate at the second proton and electron transfer step where *CHCH₂ \rightarrow *CH₂CH₂ competes against *CHCH₂ \rightarrow *CHCH₃. The second divergence is the desorption of CH₂CH₂(g) against further hydrogenation into *CH₂CH₃.

To search for optimized electrocatalysts for C₂H₂ semi-hydrogenation, computational studies, such as density functional theory (DFT) calculations, are commonly employed due to an acceptable accuracy at a relatively fast screening pace. In the past years, computational research was mainly focused on the thermocatalytic C₂H₂ semi-hydrogenation, ^{14, 69, 70} while research on the electrocatalytic counterpart is still in its infancy due to the complexity of electrochemical systems involving multiple factors such as electrolytes, pH, solvation, and applied potentials. 71-73 In 2021, Bu et al. conducted DFT studies on the (100) surfaces of Pd, Au, Ag, Ni, and Cu in electrocatalytic C₂H₂ semi-hydrogenation and identified Cu as the only metal that exhibits exothermic ("downhill") steps for the C₂H₂ adsorption, *C₂H₂ hydrogenation and C₂H₄ desorption processes (**Fig.** 3b). In 2022, Chen et al. studied the reactivity trend in electrocatalytic C₂H₂ semi-hydrogenation over 12 facecentered cubic (FCC) transition metals (TMs) including Cu, Ag, Au, Ni, Pd, Pt, Co, Rh, Ir, Ru, Os and Re.⁷⁴ They chose the free-energy change of the potential-determining step (ΔG_{PDS}) as the activity descriptor and the selectivity toward *CH2CH2 and *CH2CH2(g) as the indicator of selectivity (IOS). Based on these criteria, metals falling in the "green region" of the activity map (Fig. 3c) and selectivity map (Fig. 3d) are auspicious candidates. Among the 12 TMs, Cu is the only metal falling into the green region of both maps, indicating its potential as the state-of-the-art electrocatalyst for C₂H₂ semi-hydrogenation. Moreover, Li et al. introduced the energy difference ($\Delta \epsilon$) between the d band center of metal sites and the π orbital of C_2H_2 as a key descriptor of the π mode adsorption strength of C_2H_2 on single-site catalysts (Fig. 3e). The Specifically, they found that a reduced $\Delta \epsilon$ value corresponds to enhanced π -mode adsorption of C_2H_2 at metal sites. Using this $\Delta\epsilon$ descriptor, the authors further screened a variety of two-dimensional (2D) metal-organic frameworks (MOFs) with various coordinated metal centers (Cu, Ni, and Co) and ligands (HITP = 2,3,6,7,10,11-hexaiminotriphenylene; HHTP = 2,3,6,7,10,11-hexahydroxytriphenylene). As illustrated in **Fig. 3f**, Cu-based MOFs exhibited the lowest $\Delta\epsilon$ value, which indicates the strongest $d-\pi$ orbitals interaction and thus favorable catalysis. The experimental results are consistent with theoretical predictions, and the details are discussed in the later section. Taken cumulatively, distinct from the thermocatalytic semi-hydrogenation of C_2H_2 which employs Pd-based catalysts as state-of-the-art, these computational investigations for electrocatalytic C_2H_2 semi-hydrogenation suggest that Cu could be the potentially state-of-the-art electrocatalyst due to favorable C_2H_2 adsorption, hydrogenation, and C_2H_4 desorption. Nevertheless, current progress in computational research is still limited by relatively narrow material screening space and oversimplified models that overlooked important key features relevant to realistic reaction conditions. More comprehensive and sophisticated studies are mandatory, and we provide some detailed discussions in the prospects section.

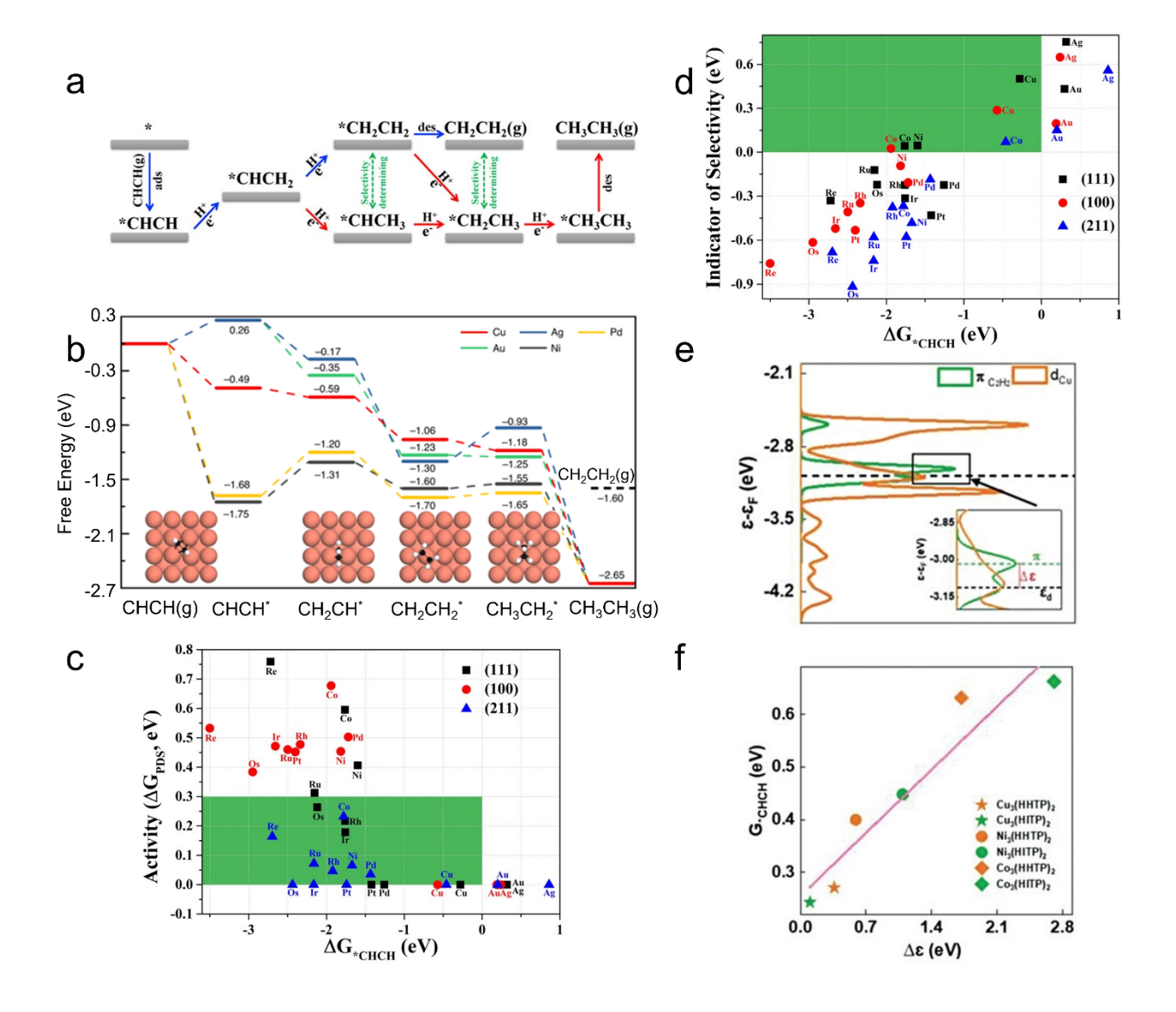


Fig. 3. a) Reaction pathways for the electrocatalytic C_2H_2 hydrogenation. Reproduced with permission.⁷⁴ Copyright 2022, American Chemical Society. b) Free-energy diagram for the C_2H_2 semi-hydrogenation to target C_2H_4 and over-hydrogenation to C_2H_6 on the (100) surfaces of Pd, Au, Ag, Ni, and Cu. Insets: most stable adsorption configurations of the intermediates on the Cu (100) surface. Reproduced with permission.⁷⁶ Copyright 2021, Nature Publishing Group. c) ΔG_{PDS} and d) IOS vs. the calculated adsorption free energy of CHCH molecule (ΔG^* CHCH) for the hydrogenation of CHCH at 0 V vs. SHE. Reproduced with permission.⁷⁴ Copyright 2022, American Chemical Society. e) Energy difference ($\Delta \varepsilon$) between the *d* band center of Cu sites and the π

orbital level of C_2H_2 . f) Correlation between $\Delta\epsilon$ and C_2H_2 adsorption free energies (G*CHCH). Reproduced with permission. ⁷⁵ Copyright 2022, Wiley-VCH.

Electrocatalysts for Semi-hydrogenation of Acetylene

Cu-based electrocatalysts As discussed in the previous section, computational studies suggest Cu as the potentially state-of-the-art for electrocatalytic C_2H_2 semi-hydrogenation. As a result, Cu-based electrocatalysts have been extensively studied in recent years. Here we summarize the performance and testing conditions of Cu-based systems in **Table 1**. For example, Bu et al. compared the electrocatalytic performances of Cu and Pd nanoparticles (NPs) in the C_2H_2 semi-hydrogenation. Cu exhibited a partial current density of 134 mA/cm² for C_2H_4 (J_{C2H4}) and a FE of C_2H_4 (J_{C2H4}) of 96% at -0.75 V vs. reversible hydrogen electrode (RHE) with a pure feed of C_2H_2 . In comparison, the J_{C2H4} and J_{C2H4} for Pd NPs were 103 mA/cm² and 83% respectively due to the competition from HER. However, during a 12-h stability test for Cu NPs at a J_{C2H4} of 50 mA/cm², the applied potential to maintain J_{C2H4} increased from -0.5 to -0.75 V while the J_{C2H4} dropped from 96% to 50%. The instability of Cu NPs agrees with literature reports that Cu-based electrocatalysts tend to suffer from leaching and surface reconstructions in electrochemical reduction reactions such as J_{C2R} and J_{C2R} compared to J_{C2R} and J_{C2R} compared to J_{C2R} compared to J

To improve the stability issue by increasing the size of Cu electrocatalysts, Bu et al. further synthesized Cu dendrites composed of aggregated Cu NPs as illustrated in **Fig. 4a**. At -0.8 V vs. RHE, the Cu dendrites achieved a j_{C2H4} of 150 mA/cm² and a FE > 93% under pure C_2H_2 flow (**Fig. 4b**). Moreover, the Cu dendrites exhibited no apparent change in applied potentials and FE_{C2H4} during the 12-h stability test. The authors also investigated the electrocatalytic performance of Cu dendrites with 1% (10,000 ppm) C_2H_2 in C_2H_4 to simulate industrial C_2H_4 -rich conditions. Considering that the low concentration of C_2H_2 in feed gas would lead to insufficient surface coverage of C_2H_2 , the authors used a flow cell with a 5×5 cm² window area to extend gas residence time. The residual concentration of C_2H_2 in 20 sccm of crude C_2H_4 was reduced to ~4 ppm with a specific selectivity of 97% for C_2H_4 . In a 120-h stability test at 40 mA, the C_2H_2 concentration was kept below 5 ppm with a stable applied cell voltage at 1.87 V. DFT calculations and operando Raman spectroscopy suggested that the outstanding

performance of Cu dendrites originated from their exothermic C_2H_2 adsorption and C_2H_4 desorption. An et al. extended the application of the Cu dendrite into a $Zn-C_2H_2$ battery. Using Zn as the anode and Cu dendrite deposited on a gas diffusion electrode as the cathode, the overall discharge reaction is C_2H_2 (g) + Zn (s) + H_2O (l) $\rightarrow C_2H_4$ (g) + ZnO (s). Under a pure C_2H_2 stream, this $Zn-C_2H_2$ battery achieved an open circuit potential of 1.14 V and a peak power density of 2.2 mV/cm². Furthermore, in simulated crude C_2H_4 (containing 1% C_2H_2), the $Zn-C_2H_2$ battery exhibited a C_2H_2 conversion of up to 99.97% at 1.2 mA/cm² and maintained stable performance during a 20-h discharge stability test. This study paved the road for the future application of electrocatalytic C_2H_2 semi-hydrogenation beyond the polymer industry.

1 μ m Cu microparticles (MPs) for electrocatalytic C_2H_2 semi-hydrogenation has been reported by Wang et al. in 2021 (**Fig. 4c**). ⁸¹ The Cu MPs afforded a current density of 29 mA/cm² and a FE_{C2H4} of 83.2% at -0.6 V vs. RHE under pure C_2H_2 flow. The coating of microporous GDL on carbon paper significantly improves the mass transport of reactants. As shown in **Fig. 4d**, Cu MPs loaded on GDL-CP exhibited notably higher current densities compared to those loaded on pristine carbon paper at all potentials from -0.4 to -0.8 V vs. RHE. Moreover, in 2022, Shi et al. reported a layered double hydroxide-derived copper electrocatalyst (LD-Cu) as illustrated in **Fig. 4e**. ⁶⁷ In 5% C_2H_2 balanced with Ar, the LD-Cu manifested an onset potential (at 10 mA/cm²) of -0.39 V vs. RHE, which is 210 mV positive than that of HER (**Fig. 4f**). At -0.6 V vs. RHE, the current density and FE was 70 mA/cm² and ~80% respectively. Under simulated C_2H_4 -rich conditions (50 sccm feed gas containing 0.5% C_2H_2 , 20% C_2H_4 balanced with Ar), the LD-Cu afforded a C_2H_2 conversion of over 99.9% using a 5×5 cm² flow cell (**Fig. 4g**). The outstanding performance of LD-Cu was attributed to the abundance of C_2H_2 0 interfaces which favor C_2H_2 adsorption and C_2H_4 desorption.

Table 1. Summary of recently developed electrocatalysts for C₂H₂ semi-hydrogenation.

Catalyst ^{ref}	Feed gas	Cell type	Current density	C ₂ H ₄	Stability
		(electrode	at the specific	FE/selectivity,	(conditions)
		area),	potential	C_2H_2	
		electrolyte		conversion	
Cu NPs ⁷⁶	20 sccm C ₂ H ₂	Flow cell	134 mA, -0.75	96% (FE)	N/A
		(1 cm²),	V vs. RHE		

		1 M KOH			
Cu dendrite ⁷⁶	20 sccm C₂H₂	Flow cell (1 cm²), 1 M KOH	150 mA, -0.8 V vs. RHE	> 93% (FE)	12 h (50 mA/cm²)
	20 sccm, 1% C ₂ H ₂ in C ₂ H ₄	Flow cell (25 cm ²), 1 M KOH	2 mA/cm ²	97% (selectivity)	120 h (40 mA)
LD-Cu ⁶⁷	10 sccm, 5% C_2H_2 in Ar	Flow cell (0.5 cm²), 1 M KOH	70 mA/cm², -0.6 V vs. RHE	74.9 ± 0.8% (FE)	N/A
	50 sccm, 0.5% C₂H₂, 20% C₂H₄ in Ar	Flow cell (25 cm²), 1 M KOH	N/A	80% (FE), 90.1% (selectivity), 99.9% (conversion)	4 h
Cu microparticles ⁸¹	4.8 sccm C ₂ H ₂	H-cell, 1 M KOH	29 mA/cm², -0.6 V vs. RHE	83.2% (FE)	100 h (12 mA/cm²)
NHC-Cu ⁸²	20 sccm C ₂ H ₂	Flow cell (1 cm²), 1 M KOH	159 mA/cm², -0.9 V vs. RHE	98% (FE)	80 h (30 mA/cm²)
	10 sccm, 1% C ₂ H ₂ in C ₂ H ₄	Flow cell (1 cm²), 1 M KOH	4 mA/cm ²	>99% (selectivity)	100 h (4 mA/cm²)
Cu ₃ (HITP) ₂ ⁷⁵	20 sccm C ₂ H ₂	Flow cell (1 cm²), 1 M KOH	124 mA/cm ² , -0.9 V vs. RHE	99.3% (FE)	25 h (30 mA/cm2)
	10 sccm, 1% C ₂ H ₂ in C ₂ H ₄	Flow cell (25 cm²), 1 M KOH	N/A	99.99% (conversion)	13 h (2.2 mA/cm²)
Ag nanowire ⁶⁸	20 sccm C ₂ H ₂	Flow cell (1 cm²), 1 M KOH	217 mA/cm ² , -0.85 V vs. RHE	99 % (FE)	120 h (10 mA/cm²)
	10 sccm, 1% C ₂ H ₂ in C ₂ H ₄	Flow cell (25 cm²), 1 M KOH	2.2 mA/cm², N/A	99 % (selectivity), 99.8% (conversion)	20 h (2.2 mA/cm²)
Ag NPs ⁸³	20 sccm C ₂ H ₂	Flow cell, (1 cm²), 1 M KOH+ D2O	100 mA/cm ² , -0.9 V vs. RHE	99.3% (FE C ₂ H ₂ D ₂)	N/A
	N/A	Flow cell (25 cm²), 1 M KOH+ D2O	N/A	95% (FE C ₂ H ₂ D ₂)	40 h (100 mA)
SA-Ni-NC ⁸⁴	20 sccm C ₂ H ₂	Flow cell (1 cm²), 1 M KOH	-92.2 mA/cm ² -0.6 V vs. RHE	91.3% (FE)	45 h (-30 mA/cm²)
	10 sccm, 1% C ₂ H ₂ in C ₂ H ₄	Flow cell (25 cm²), 1 M KOH	-1.6 mA/cm ²	97.4% (conversion)	500 min (40 mA)
CoPc ⁸⁵	20 sccm C ₂ H ₂	Flow cell	150.8 mA/cm ²	96%(FE)	N/A

	(1 cm²), 1 M KOH	-0.7 V vs. RHE		
10 sccm, 1% C ₂ H ₂ in C ₂ H ₄	Flow cell (25 cm²), 1 M KOH	2.8 mA/cm ²	99.5% (conversion)	40 h (2.8 mA/cm²)

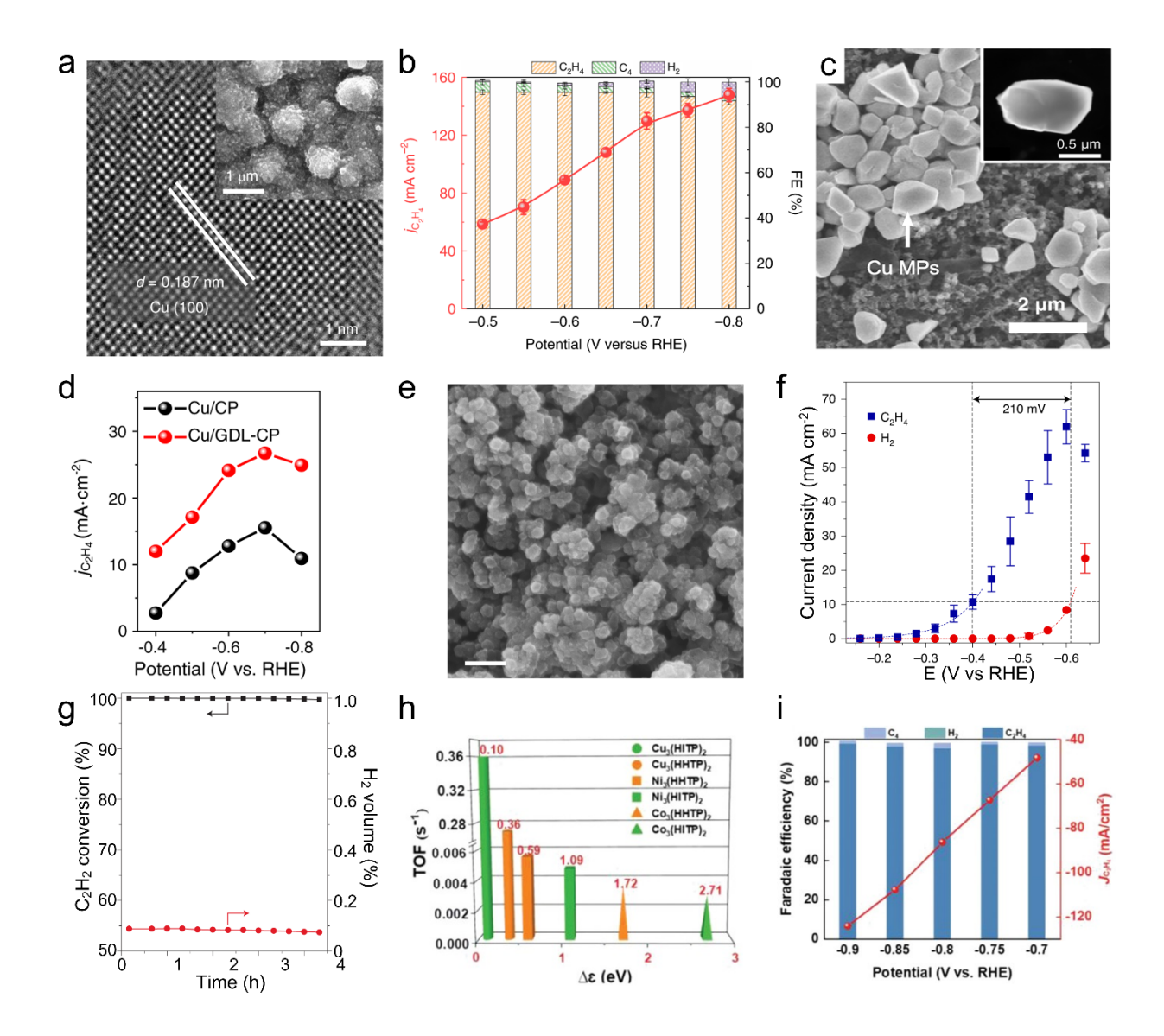


Fig. 4. a) The aberration-corrected transmission electron microscope (TEM) and scanning electron microscopy (SEM) (inset) images of the Cu dendrites. b) j_{C2H4} and FE_{C2H4} versus the potentials in 1 M KOH obtained on the Cu dendrites. Reproduced with permission.⁷⁶ Copyright 2021, Nature Publishing Group. c) SEM and High-angle annular dark-field scanning transmission electron microscopy (HAADF-STEM) (inset) images of Cu MPs. d)

Comparison between the j_{C2H4} on the Cu MPs loaded on pristine carbon papers (Cu/CP) and Cu MPs loaded on GDL-CP (Cu/GDL-CP). Reproduced with permission.⁸¹ Copyright 2021, Nature Publishing Group. e) SEM image of LD-Cu on the microporous layer. Scale bar, 200 nm. f) Partial current densities for C_2H_4 and H_2 production obtained on LD-Cu versus applied potentials. g) C_2H_2 conversion and H_2 volume percentage versus time under simulated C_2H_4 -rich conditions. Reproduced with permission.⁶⁷ Copyright 2021, Nature Publishing Group. h) TOF versus $\Delta \varepsilon$ of 2D MOFs. i) FE_{C2H4} and j_{C2H4} of $Cu_3(HITP)_2$ catalysts versus the potentials. Reproduced with permission.⁷⁵ Copyright 2022, Wiley-VCH.

In addition to NPs and microparticles, Cu-based metal complexes and MOFs have been studied. For example, Zhang et al. developed a series of N-heterocyclic carbene (NHC)-metal complexes (Cu, Ag, Au, and Pd) for electrocatalytic C₂H₂ semi-hydrogenation.⁸² According to their DFT calculations, NHC-Cu is the most promising candidate among all the NHC-metal complexes, with a low free energy barrier (0.02 eV) for semihydrogenation and exothermic C₂H₄ desorption process (-0.07 eV). The Ab initio prediction was further confirmed by experimental results, where NHC-Cu showed a FE_{C2H4} of ≥98% under pure C₂H₂ feed. With a crude C₂H₄ feed flow containing only 1% C₂H₂, NHC-Cu still exhibited a C₂H₄-specific selectivity of >99%, an SV of 9.6 \times 10⁵ mL/g_{cat}/h, a turnover frequency (TOF) of 2.1 \times 10⁻² s⁻¹ and a continuous output of C₂H₄ with only ~30 ppm C₂H₂ during a 100-h stability test. Bader charge analyses revealed charge transfer from NHC ligands to the Cu center. The electron-rich Cu sites facilitated the adsorption of electrophilic C₂H₂ and desorption of nucleophilic C₂H₄ and subsequently suppressed side reactions. Furthermore, in 2022, Li et al. compared the activity of a series of 2D MOFs with different metal atoms (Ni, Co, and Cu) and ligands (HITP and HHTP). 75 As discussed in the computational insights section, $\Delta \varepsilon$ between the d-band center of the metal and π orbital of alkynes was selected as the energetic descriptor for the semi-hydrogenation activities of electrocatalyst candidates. Consequently, Cu₃(HITP)₂, with the smallest Δε (0.10eV), demonstrated the highest TOF among all its metal analogs (Fig. 4h) together with a high j_{C2H4} of -124 mA/cm² and a large FE_{C2H4} of 99.3% at -0.9 V vs. RHE (Fig. 4i). In a crude C₂H₄ condition containing 1% C₂H₂, a C₂H₂ conversion of ≈99.99% was achieved and maintained over a 13-h stability measurement at 2 mA/cm².

Non-Cu-based electrocatalysts Despite the outstanding activity and C_2H_4 specific selectivity, Cu-based electrocatalysts suffer from some intrinsic problems, such as the stability issue as mentioned in the previous section, hindering their practical applications. In addition, C-C coupling on Cu-based electrocatalysts in C_2H_2 semi-hydrogenation produces unwanted 1,3-butadiene and green oil. In order to alleviate C-C coupling, Bai et al. synthesized silver nanowires (Ag NWs) as illustrated in **Fig. 5a.**⁶⁸ At -0.2 V vs. RHE, the FE of 1,3-butadiene was only 2.1% on Ag NWs in comparison to that of 41.2% on Cu NPs. DFT calculations and *in situ* Raman spectroscopy indicate that the weak endothermic C_2H_2 adsorption on Ag (111) surfaces intrinsically inhibited the oligomerization of C_2H_2 molecules. Moreover, the Ag NWs exhibited a j_{C2H_4} of 217 mA/cm² at -0.85 V vs. RHE under pure C_2H_2 . Under crude C_2H_4 , the Ag NWs reached a 98% C_2H_2 conversion and ~99% C_2H_4 specific selectivity at 2.2 mA/cm² as shown in **Fig. 5b.** In 2022, Chang et al. reported the application of Ag NPs in electrosynthesis of deuterated ethylene ($C_2H_2D_2$) from C_2H_2 (**Fig. 5c**). ⁸³ Using 1 M KOH D_2O solution as both the electrolyte and deuterium (D) source, the Ag NPs exhibited a FE_{C2H2D2} of 99.3% at -0.6 V vs. RHE and a partial current density of 100 mA/cm² at -0.9 V vs. RHE (**Fig. 5d**). During a 40-h stability assessment in a 25 cm² flow cell, the Ag NPs exhibited FE_{C2H2D2} of >95% and a constant $C_2H_2D_2$ production rate of 1.44 × 10³ mmol/h/g_{cat}.

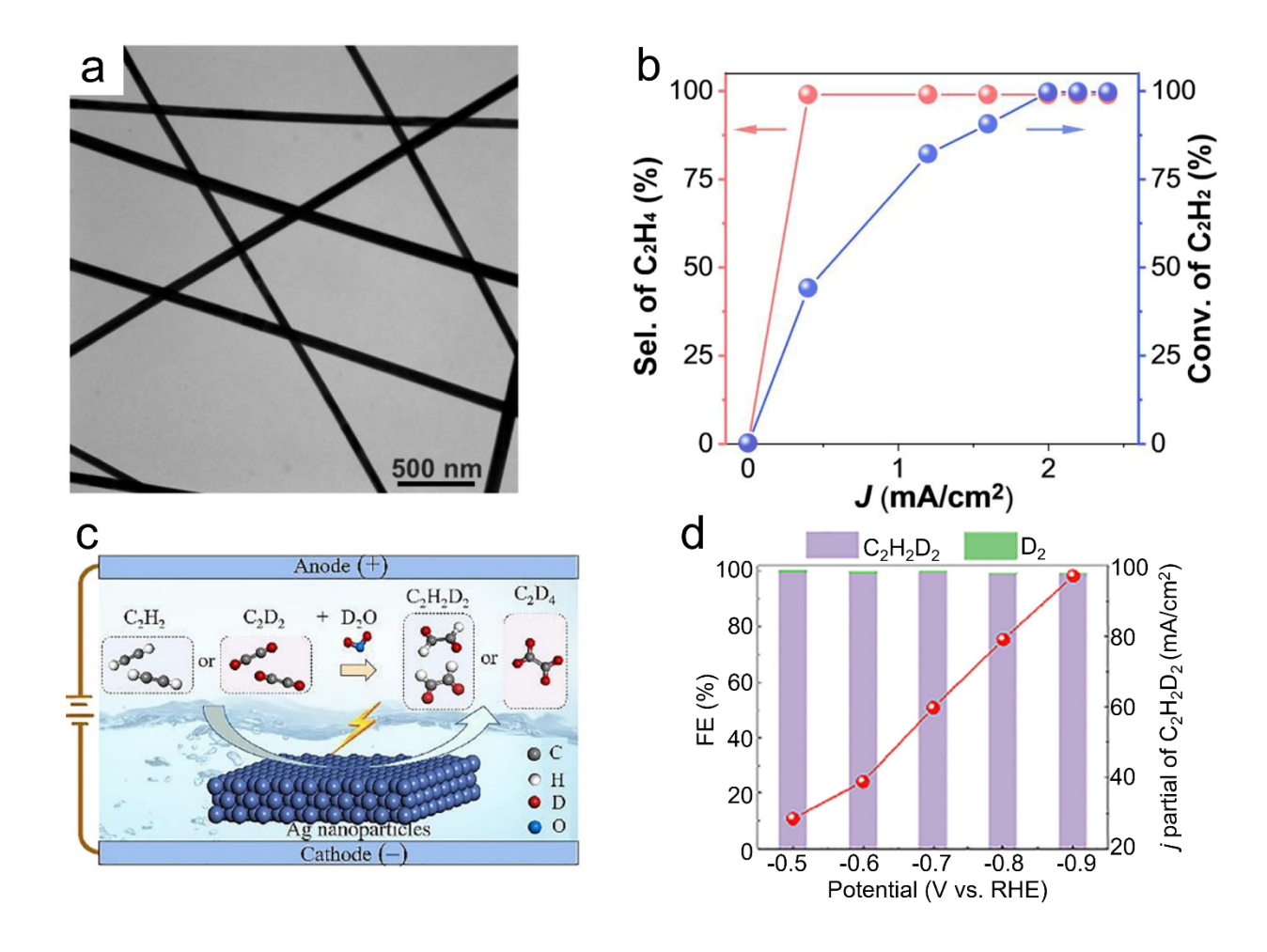


Fig. 5. a) TEM image of Ag NWs. b) Specific selectivity of C_2H_4 and C_2H_2 conversion versus current densities at a flow rate of 10 sccm in crude C_2H_4 . Reproduced with permission.⁶⁸ Copyright 2022, Chinese Chemical Society. c) Schematic demonstration of electrocatalytic deuteration of C_2H_2 with Ag NPs. d) FE_{C2H2D2} and $C_2H_2D_2$ partial current density of Ag NPs at -0.5 to -0.9 V vs. RHE. Reproduced with permission.⁸³ Copyright 2022, Elsevier B.V. on behalf of Chinese Chemical Society and Institute of Materia Medica, Chinese Academy of Medical Sciences.

Single-site catalysts serve as an alternative strategy to suppress C-C coupling due to moderate π -mode adsorption and isolated active sites. In 2022, Ma et al. synthesized single-atom nickel dispersed in N-doped carbon (SA-Ni-NC) with Ni–N₄ coordination as an electrocatalyst for C_2H_2 semi-hydrogenation (**Fig. 6a**). ⁸⁴ Under pure C_2H_2 stream, SA-Ni-NC achieved a high FE of 91.3% (**Fig. 6b**) and a j_{C2H4} of 92.2 mA/cm² (**Fig. 6c**) at -0.6 V vs. RHE. *In situ* Raman spectroscopy captured the moderate π -mode adsorption of C_2H_4 on Ni single sites from

0 to -0.6 V vs. RHE. The π -mode adsorption favored a rapid C_2H_4 desorption in agreement with the DFT results of an exothermal step by 0.23 eV. Moreover, Liu et al. developed metal phthalocyanines (MPc, M= Co, Cu, Zn) which is another form of single-site catalyst for C_2H_2 semi-hydrogenation. Specifically, a metal Pc is a molecular complex with a single metal center coordinated by Pc ligands as illustrated in Fig. 6d (inset). Among the MPcs, CoPc exhibited the best performance with a FE of 96% at -0.4 V vs. RHE and a j_{C2H4} of 92.2 mA/cm² at -0.7 V vs. RHE in pure C_2H_2 stream (Fig. 6e and 6f). In situ Raman and DFT demonstrated that while all the MPcs exhibit mild adsorption of C_2H_x species on isolated metal atoms, only CoPc manifests an exothermic hydrogenation step from C_2H_2 into C_2H_2 intermediates due to the intrinsic electronic structure of Co centers. In addition, under simulated crude C_2H_4 stream, CoPc manifested > 99.2% C_2H_2 conversion and 40-h durability at 2.8 mA/cm².

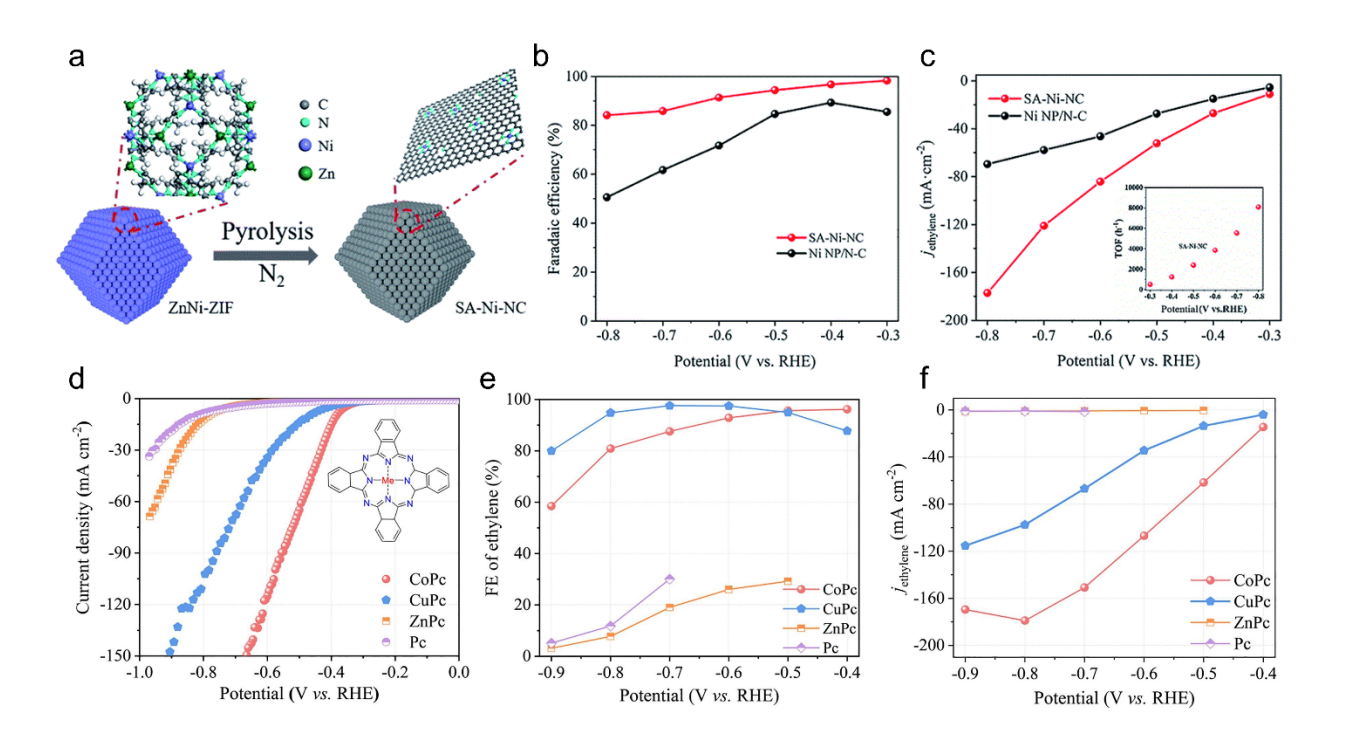


Fig. 6. a) Schematic illustration of the synthesis process of SA-Ni-NC. b) FE and c) partial current density of C_2H_4 for SA-Ni-NC at different potentials. Inset: TOF. Reproduced with permission.⁸⁴ Copyright 2022, The Royal Society of Chemistry. d) LSV curves of MPc catalysts (inset) in a pure C_2H_2 atmosphere. e) FE and f) Partial

current density of C_2H_4 for MPc catalysts at various potentials. Reproduced with permission.⁸⁵ Copyright 2022, Elsevier.

Perspectives, Challenges, and Opportunities of Electrocatalytic Semi-hydrogenation of C₂H₂

Electrocatalytic C₂H₂ semi-hydrogenation coupled with renewable energy sources offers a potentially more economical, sustainable, and selective alternative to the traditional thermocatalytic schemes for producing polymer-grade C₂H₄ feed. In the past couple of years, breakthroughs in electrocatalytic C₂H₂ semi-hydrogenation have been made owing to the maturity of GDL-based technologies and the development of a wide range of novel electrocatalysts including NPs, microscale structures, 2D structures, metal complexes, and single-site catalysts. In the meantime, challenges and opportunities co-exist in the current electrocatalytic systems. In this section, we provide prospects based on the discussions of recent publications and propose tools and strategies to overcome corresponding challenges for the future development of advanced systems of electrocatalytic C₂H₂ semi-hydrogenation.

i) *Comprehensive computational insights*: Electrocatalytic reactions at the solid-gas-electrolyte interface proceed via the adsorption of charge transfer intermediates, followed by the desorption of products into the electrolyte. The complexity of electrochemical interfaces has not been considered thoroughly in many publications. For example, how the distribution of ions within the Helmholtz layer and the solvation could impact the interfacial electrokinetic has often been neglected, not to mention the potential structural evolution of catalysts during the reaction and often over-simplified models when considering the catalytic sites. While this has been a common issue for many electrocatalytic studies and needs to be addressed by developing more sophisticated models and computational approaches, ^{73, 86, 87} systematic computational studies for electrocatalytic C₂H₂ semi-hydrogenation have not been investigated in a rigorous manner as compared to other electrocatalytic reactions. For example, the work by Bu et al. screened limited materials space, restricted to the (100) surfaces of 5 metals for electrocatalytic C₂H₂ semi-hydrogenation ⁷⁶, and the DFT study by Chen et al. only covered FCC metals. ⁷⁴ Questions such as whether Cu is state-of-the-art would require more

comprehensive computational studies in extended materials space, considering various facets including the (100), (111), (110), and high-index facets of TMs and post-TMs. The commonly adopted volcano plots based on Sabatier's principle as references for designing electrocatalysts for reactions such as HER^{88, 89}, and nitrogen reduction reaction (NRR), $^{90, 91}$ need to be developed. Finding appropriate reaction descriptors such as the $\Delta\epsilon$ and binding energies of specific intermediates can increase the efficiency of establishing such volcano plots or heat maps. $^{75, 92, 93}$ In addition, single atoms exhibit distinct electronic structures and coordination environments compared with their bulk and nanoscale counterparts. 94 Therefore, conducting computational screening of metal single atoms would facilitate designing single-atom electrocatalysts for C_2H_2 semi-hydrogenation.

ii) Stability and selectivity of electrocatalysts: Based on current studies, Cu is considered the state-of-the-art catalyst for electrocatalytic C₂H₂ semi-hydrogenation before more comprehensive computational and experimental screenings. Albeit the outstanding performances, two drawbacks for Cu-based electrocatalysts have been frequently noticed. First, Cu may not be stable and could consistently experience structural evolution via a series of stochastic events, e.g., migration, dissolution, and re-deposition in many electrocatalytic reactions. 77-79 The most common strategy to stabilize Cu structures is to design microscale Cu-based electrocatalysts. 45, 67, 76, 81 Nevertheless, the increased size inevitably reduces the percentage of surface-active sites, leading to compromised activity. To further develop robust and high-performing Cu-based electrocatalysts, their dynamic morphology and coordination environment evolution need to be investigated and interrogated, which necessitates the use of in situ and operando techniques such as in situ STEM and X-ray absorption spectroscopy (XAS). The second problem is the C-C coupling into 1,3-butadiene and green oil. Single-site catalysts with isolated active sites and moderate π-adsorption of C₂H_X species could be a viable solution. Note that single-site catalysts not only include SACs but also include single-atom alloys, metal complexes, and MOFs with single metal atom centers. In thermocatalysis, Pd-based single-site catalysts have been intensely investigated for improving the C₂H₄ selectivity against oligomerization^{6, 26, 28, 95, 96} and Cu-based SAC has also been studied at elevated reaction temperatures.⁹⁷ In previous section, we have discussed single-site catalysts including NHC-Cu, SA-Ni-NC, and CoPc and they exhibited high FE (>90%) with minimum multi-carbon products.

When designing single-site electrocatalysts, conductive supports such as N-doped carbon need to be considered rather than oxide supports typically employed in SACs for thermocatalysis. We also would like to mention that 1,3-butadiene and green oil products are readily dissolved in electrolytes in electrocatalytic systems and can be directly quantified through techniques such as nuclear magnetic resonance (NMR).

iii) Comparison with the thermocatalytic C_2H_2 semi-hydrogenation: Two selectivity parameters of C_2H_4 need to be specified here: the specific selectivity and the FE. Specific selectivity (**Equation 2**) is commonly used in thermocatalytic systems, and it reflects the production rate of C_2H_4 against other products (mainly C_2H_6):

specific selectivity =
$$\frac{C_{C2H4,out}}{C_{C2H2,in} - C_{C2H2,out}}$$
(2)

, where C_x refers to the concentration of species x entering (in) or leaving (out) the reactor. For the electrocatalytic systems, due to the *in situ* generation and consumption of hydrogen source, the specific selectivity tends to be intrinsically high (>95%) as we have discussed previously. However, it does not consider the competition of HER which is the major side reaction for electrochemical reductions. FE (**Equation 3**) describes the efficiency of electrons transferred to the system participating in a target electrochemical reaction and it is defined as the percentage of current participated in a specific reaction among total applied current density:

$$FE = \frac{j_{C2H4}}{I} \times 100\% (3)$$

, where J is the total current density and j_{C2H4} is the partial current density of C_2H_4 . Usually, FE instead of the specific selectivity is employed in electrochemical systems. However, under simulated industrial conditions where only scarce C_2H_2 ($\leq 1\%$) exists in the feed, FE may not be an accurate descriptor for selectivity since HER could be dominant. Therefore, both specific selectivity and FE are recommended to be reported for a precise and comprehensive description of C_2H_4 selectivity in electrocatalytic C_2H_2 semi-hydrogenation.

Other commonly reported parameters in thermocatalytic systems include conversion, SV, and turnover frequency (TOF). In the electrocatalytic C_2H_2 semi-hydrogenation system, these parameters can be calculated as **Equation 4**, **5** and **6** respectively:

$$Conversion = \left(1 - \frac{C_{C2H2,in}}{C_{C2H2,out}}\right) \times 100\% (4)$$

$$SV = \frac{v_0}{m} (5)$$

$$TOF = \frac{I_{C2H4} / nF}{m \times \omega / M}$$
(6)

, where v_0 is the volumetric flow rate of feeding gas in ml/h, m is the weight of catalyst in g, n is the number of electrons transferred for product formation (n=2 for C₂H₄), ω is the mass fraction of metal (e.g. Cu) in the catalyst and M is the molecular weight of the metal in g/mol.^{75, 76, 84} For some electrochemical systems that commonly employ H-cells, e.g., CO₂RR, conversion and SV have no significant meaning due to the limited solubility of the feed gas which leads to a very small portion of feed gas that is reacted. For systems employing flow cells such as C₂H₂ semi-hydrogenation, conversion and SV values can be comparable to the thermocatalytic counterparts. As we discussed previously, most studies reported close to 100% conversions under simulated crude C₂H₄ streams. The reported SV values also match those of thermocatalysis. For example, the Cu dendrites achieved 9.6 × 10⁴ ml/g_{cat}/h, ⁷⁶ NHC-Cu achieved 9.6 × 10⁵ mL/g_{cat}/h, ⁸² and SA-Ni-NC exhibited 2.4 × 10⁴ mL/g_{cat}/h. h. ⁸⁴ TOF is a parameter measuring the intrinsic activity of a catalyst and is commonly used in both thermocatalytic and electrocatalytic systems. ^{29, 75, 85} In summary, parameters including specific selectivity, FE, conversion, SV and TOF, are important and mandatory to make comprehensive comparisons between electrocatalytic and thermocatalytic systems for C₂H₂ semi-hydrogenation.

iv) C_2H_2 Solubility and practical applications: The limited solubility of C_2H_2 in water is the key factor inhibiting the practical application of electrocatalytic C_2H_2 semi-hydrogenation systems and the extremely low concentration of C_2H_2 in the feed gas exacerbates this challenge. In comparison, despite a similar solubility of

1450 mg/L at 27 °C for CO₂,⁹⁸ CO₂RR can achieve high current densities (> 100 mA/cm²) with a pure feed of CO₂,^{99, 100} Application of GDL-base flow cells can significantly alleviate the solubility issue to some extent yet not sufficient for practical applications. For example, despite reasonable currents (>50 mA) in 25 cm² flow cells having been achieved, the current densities are typically low (< 5 mA/cm²) due to the extra-large electrode surface and a subsequent significant amount of catalyst loading. In addition, considering relatively overpotentials (> 1 V) are applied for this system, the energy efficiency is deemed to be low. Industrial application of electrocatalytic C₂H₂ hydrogenation may require the use of a series of MEA stacks. Also, in practical flow cell MEA, the movement of water from the electrolyte can lead to flooding of the GDE, which necessitates the quantification of water transport at the cathode.^{101, 102} More importantly, how to effectively and economically incorporate the electrocatalytic system with the existing C₂H₄ synthesis and purification schemes remains unsolved, calling for a comprehensive techno-economic analysis and life cycle assessment.

v) Front-end and tail-end configurations: Industrial C_2H_2 semi-hydrogenation conditions can be categorized into Front-end and tail-end configurations depending on the position of the hydrogenation reactor relative to the cold box. Tail-end configuration accounts for 70% of global units while front-end accounts for the rest 30%. 103 Owing to the ambient operating conditions and independence of H_2 feed, the electrocatalytic system represents a suitable constituent of the tail-end configurations which create a low-temperature and H_2 lean environment for C_2H_2 semi-hydrogenation. Nevertheless, tail-end configurations require additional attention on the C-C coupling issue due to the H_2 lean conditions.

vi) Beyond C_2H_2 - electrocatalytic semi-hydrogenation of alkynes: Selective hydrogenation of alkynes beyond C_2H_2 opens up far-reaching opportunities in the fine chemical industry due to wide applications of tailorable alkenes in drug synthesis and chemical science. $^{104-106}$ C_2H_2 can serve as a model molecule to understand the reactivity of electrocatalysts in the semi-hydrogenation of more complex alkynes. For example, Gao et al. have used C_2H_2 semi-hydrogenation as a probe reaction to screen the performance of Pd-base electrocatalysts. 107 In addition, the Cu dendrites have achieved near 100% conversion of propyne and butyne in crude propylene and

1,3-butadiene streams.⁷⁶ While a detailed discussion of electrocatalytic systems to alkynes other than acetylene is beyond the scope of this manuscript, we recommend relevant literature as references.¹⁰⁷⁻¹⁰⁹

vii) *Additional concerns and potential solutions*: The electrocatalysts we have introduced so far work under alkaline conditions with operation time limited to 120 h. Therefore, how to design an electrocatalyst working under neutral or acidic electrolytes and how to further prolong operation time to industrial requirements (10000 h) remain challenging. The potential solution is to expand the catalyst system into multi-element materials. Compared with single-metal catalysts, multi-element electrocatalysts synthesized from doping, alloying, or coating exhibit tunable physical and chemical properties from controllable compositions and ordering. However, due to the complexity of compositions and structures, we recommend a thorough study of reaction mechanisms on pure metal surfaces before the rational design of multi-element electrocatalysts. This would require a combination of in situ or operando experimental techniques such as Fourier-transform infrared spectroscopy (FTIR) 43,81,113 and Raman spectrometry 76,82 with computational studies such as DFT. 114,115

Conclusion

Recent years have witnessed substantial progress in electrocatalytic C_2H_2 semi-hydrogenation, which is deemed to be a promising alternative to conventional thermocatalytic systems to produce polymer-grade C_2H_4 feed. Electrocatalytic C_2H_2 semi-hydrogenation systems have the merits of higher C_2H_4 selectivity, a greener hydrogen source, and ambient operating conditions. Herein, we have summarized and discussed recent progress in the development of electrocatalytic C_2H_2 semi-hydrogenation, highlighting the reactor design, computational studies, and development of electrocatalysts. We then provide prospects and outlooks on potential strategies to address challenges in this field. We envision that with continued research and development, electrocatalytic C_2H_2 semi-hydrogenation could have a substantial impact on the sustainability of our global energy and chemical economy.

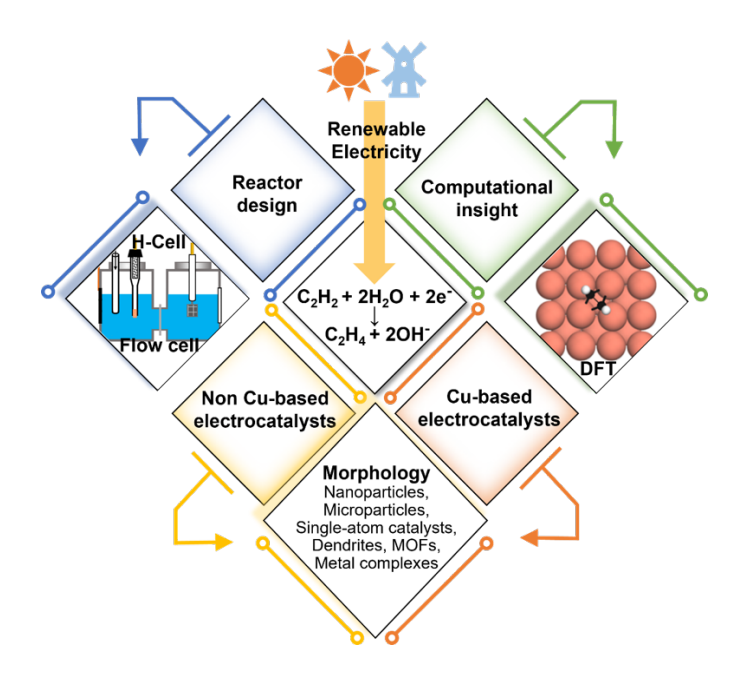
Conflict of Interest

The authors declare no conflict of interest.

Funding Information

This work was supported by the US National Science Foundation (CHE-2102363).

Table of Contents Graphic



References

- 1. Aggarwal, S. L.; Sweeting, O. J. Polyethylene: Preparation, Structure, And Properties. *Chem. Rev.* **1957**, 57, 665-742.
- 2. Geyer, R.; Jambeck, J. R.; Law, K. L. Production, use, and fate of all plastics ever made. *Sci. Adv.* **2017**, 3, e1700782.
- 3. Turner John, A. Sustainable Hydrogen Production. *Science* **2004**, 305, 972-974.
- 4. McCue, A. J.; Anderson, J. A. Recent advances in selective acetylene hydrogenation using palladium containing catalysts. *Front. Chem. Sci. Eng.* **2015**, 9, 142-153.
- 5. Vilé, G.; Almora-Barrios, N.; Mitchell, S.; López, N.; Pérez-Ramírez, J. From the Lindlar Catalyst to Supported Ligand-Modified Palladium Nanoparticles: Selectivity Patterns and Accessibility Constraints in the Continuous-Flow Three-Phase Hydrogenation of Acetylenic Compounds. *Chem. Eur. J.* **2014**, 20, 5926-5937.
- 6. Pei, G. X.; Liu, X. Y.; Wang, A.; Lee, A. F.; Isaacs, M. A.; Li, L.; Pan, X.; Yang, X.; Wang, X.; Tai, Z.; Wilson, K.; Zhang, T. Ag Alloyed Pd Single-Atom Catalysts for Efficient Selective Hydrogenation of Acetylene to Ethylene in Excess Ethylene. *ACS Catal.* **2015**, 5, 3717-3725.
- 7. García-Mota, M.; Gómez-Díaz, J.; Novell-Leruth, G.; Vargas-Fuentes, C.; Bellarosa, L.; Bridier, B.; Pérez-Ramírez, J.; López, N. A density functional theory study of the 'mythic' Lindlar hydrogenation catalyst. *Theor. Chem. Acc.* **2011**, 128, 663-673.
- 8. Gonçalves, L. P. L.; Wang, J.; Vinati, S.; Barborini, E.; Wei, X.-K.; Heggen, M.; Franco, M.; Sousa, J. P. S.; Petrovykh, D. Y.; Soares, O. S. G. P.; Kovnir, K.; Akola, J.; Kolen'ko, Y. V. Combined experimental and theoretical study of acetylene semi-hydrogenation over Pd/Al₂O₃. *Int. J. Hydrogen Energy* **2020**, 45, 1283-1296.
- 9. Zhang, H.; Wang, Y.; Cao, J.; Kang, P.; Tang, Q.; Ma, M. Highly Dispersed PdNPs/ α -Al₂O₃ Catalyst for the Selective Hydrogenation of Acetylene Prepared with Monodispersed Pd Nanoparticles. *Catalysts* **2017**, 7, 128.
- 10. Zhou, S.; Kang, L.; Xu, Z.; Zhu, M. Catalytic performance and deactivation of Ni/MCM-41 catalyst in the hydrogenation of pure acetylene to ethylene. *RSC Advances* **2020**, 10, 1937-1945.
- 11. McCue, A. J.; Guerrero-Ruiz, A.; Rodríguez-Ramos, I.; Anderson, J. A. Palladium sulphide A highly selective catalyst for the gas phase hydrogenation of alkynes to alkenes. *J. Catal.* **2016**, 340, 10-16.
- 12. Sholl, D. S.; Lively, R. P. Seven chemical separations to change the world. *Nature* **2016**, 532, 435-437.
- 13. Zhang, P.; Zhong, Y.; Zhang, Y.; Zhu, Z.; Liu, Y.; Su, Y.; Chen, J.; Chen, S.; Zeng, Z.; Xing, H.; Deng, S.; Wang, J. Synergistic binding sites in a hybrid ultramicroporous material for one-step ethylene purification from ternary C2 hydrocarbon mixtures. *Sci. Adv.* **2022**, 8, eabn9231.
- 14. Jørgensen, M.; Grönbeck, H. Selective Acetylene Hydrogenation over Single-Atom Alloy Nanoparticles by Kinetic Monte Carlo. *J. Am. Chem. Soc.* **2019**, 141, 8541-8549.
- 15. Fu, X.; Liu, J.; Kanchanakungwankul, S.; Hu, X.; Yue, Q.; Truhlar, D. G.; Hupp, J. T.; Kang, Y. Two-Dimensional Pd Rafts Confined in Copper Nanosheets for Selective Semihydrogenation of Acetylene. *Nano Lett.* **2021**, 21, 5620-5626.
- 16. Sárkány, A.; Weiss, A. H.; Guczi, L. Structure sensitivity of acetylene-ethylene hydrogenation over Pd catalysts. *J. Catal.* **1986**, 98, 550-553.
- 17. Sárkány, A.; Weiss, A. H.; Szilágyi, T.; Sándor, P.; Guczi, L. Green oil poisoning of a Pd/a1203 acetylene hydrogenation catalyst. *Appl. Catal.* **1984**, 12, 373-379.
- 18. Zhang, J.; Sui, Z.; Zhu, Y.-A.; Chen, D.; Zhou, X.; Yuan, W. Composition of the Green Oil in Hydrogenation of Acetylene over a Commercial Pd-Ag/Al₂O₃ Catalyst. *Chem. Eng. Technol.* **2016**, 39, 865-873.
- 19. Barelli, L.; Bidini, G.; Gallorini, F.; Servili, S. Hydrogen production through sorption-enhanced steam methane reforming and membrane technology: A review. *Energy* **2008**, 33, 554-570.
- 20. Burch, R. Gold catalysts for pure hydrogen production in the water–gas shift reaction: activity, structure and reaction mechanism. *Phys. Chem. Chem. Phys.* **2006**, 8, 5483-5500.
- 21. Katebah, M.; Al-Rawashdeh, M. m.; Linke, P. Analysis of hydrogen production costs in Steam-Methane Reforming considering integration with electrolysis and CO₂ capture. *Cleaner Engineering and Technology* **2022**, 10, 100552.
- 22. Scholz, W. H. Processes for industrial production of hydrogen and associated environmental effects. *Sep. Purif. Technol.* **1993**, 7, 131-139.
- Wang, Z.; Li, L.; Zhang, G. Life cycle greenhouse gas assessment of hydrogen production via chemical looping combustion thermally coupled steam reforming. *J. Clean. Prod.* **2018**, 179, 335-346.
- 24. McGown, W. T.; Kemball, C.; Whan, D. A. Hydrogenation of acetylene in excess ethylene on an alumina-supported palladium catalyst at atmospheric pressure in a spinning basket reactor. *J. Catal.* **1978**, 51, 173-184.

- 25. Lou, B.; Kang, H.; Yuan, W.; Ma, L.; Huang, W.; Wang, Y.; Jiang, Z.; Du, Y.; Zou, S.; Fan, J. Highly Selective Acetylene Semihydrogenation Catalyst with an Operation Window Exceeding 150 °C. ACS Catal. **2021**, 11, 6073-6080.
- 26. Kyriakou, G.; Boucher Matthew, B.; Jewell April, D.; Lewis Emily, A.; Lawton Timothy, J.; Baber Ashleigh, E.; Tierney Heather, L.; Flytzani-Stephanopoulos, M.; Sykes, E. C. H. Isolated Metal Atom Geometries as a Strategy for Selective Heterogeneous Hydrogenations. *Science* **2012**, 335, 1209-1212.
- Liu, S.; Li, Y.; Yu, X.; Han, S.; Zhou, Y.; Yang, Y.; Zhang, H.; Jiang, Z.; Zhu, C.; Li, W.-X.; Wöll, C.; Wang, Y.; Shen, W. Tuning crystal-phase of bimetallic single-nanoparticle for catalytic hydrogenation. *Nat. Commun.* **2022**, 13, 4559.
- 28. Feng, Q.; Zhao, S.; Wang, Y.; Dong, J.; Chen, W.; He, D.; Wang, D.; Yang, J.; Zhu, Y.; Zhu, H.; Gu, L.; Li, Z.; Liu, Y.; Yu, R.; Li, J.; Li, Y. Isolated Single-Atom Pd Sites in Intermetallic Nanostructures: High Catalytic Selectivity for Semihydrogenation of Alkynes. *J. Am. Chem. Soc.* **2017**, 139, 7294-7301.
- 29. Wu, P.; Tan, S.; Moon, J.; Yan, Z.; Fung, V.; Li, N.; Yang, S.-Z.; Cheng, Y.; Abney, C. W.; Wu, Z.; Savara, A.; Momen, A. M.; Jiang, D.-e.; Su, D.; Li, H.; Zhu, W.; Dai, S.; Zhu, H. Harnessing strong metal—support interactions via a reverse route. *Nat. Commun.* **2020**, 11, 3042.
- 30. Yan, Z.; Yao, B.; Hall, C.; Gao, Q.; Zang, W.; Zhou, H.; He, Q.; Zhu, H. Metal–Metal Oxide Catalytic Interface Formation and Structural Evolution: A Discovery of Strong Metal–Support Bonding, Ordered Intermetallics, and Single Atoms. *Nano Lett.* **2022**, 22, 8122-8129.
- 31. Teschner, D.; Borsodi, J.; Wootsch, A.; Révay, Z.; Hävecker, M.; Knop-Gericke, A.; Jackson, S. D.; Schlögl, R. The Roles of Subsurface Carbon and Hydrogen in Palladium-Catalyzed Alkyne Hydrogenation. *Science* **2008**, 320, 86-89.
- 32. Zhang, L.; Zhou, M.; Wang, A.; Zhang, T. Selective Hydrogenation over Supported Metal Catalysts: From Nanoparticles to Single Atoms. *Chem. Rev.* **2020**, 120, 683-733.
- 33. Vilé, G.; Albani, D.; Almora-Barrios, N.; López, N.; Pérez-Ramírez, J. Advances in the Design of Nanostructured Catalysts for Selective Hydrogenation. *ChemCatChem* **2016**, 8, 21-33.
- 34. Meng, F.; Zhong, H.; Bao, D.; Yan, J.; Zhang, X. In Situ Coupling of Strung Co₄N and Intertwined N–C Fibers toward Free-Standing Bifunctional Cathode for Robust, Efficient, and Flexible Zn–Air Batteries. *J. Am. Chem. Soc.* **2016**, 138, 10226-10231.
- 35. Meng, F.-L.; Liu, K.-H.; Zhang, Y.; Shi, M.-M.; Zhang, X.-B.; Yan, J.-M.; Jiang, Q. Recent Advances toward the Rational Design of Efficient Bifunctional Air Electrodes for Rechargeable Zn–Air Batteries. *Small* **2018**, 14, 1703843.
- 36. Gao, Y.; Xue, Y.; Qi, L.; Xing, C.; Zheng, X.; He, F.; Li, Y. Rhodium nanocrystals on porous graphdiyne for electrocatalytic hydrogen evolution from saline water. *Nat. Commun.* **2022**, 13, 5227.
- 37. Cheng, N.; Stambula, S.; Wang, D.; Banis, M. N.; Liu, J.; Riese, A.; Xiao, B.; Li, R.; Sham, T.-K.; Liu, L.-M.; Botton, G. A.; Sun, X. Platinum single-atom and cluster catalysis of the hydrogen evolution reaction. *Nat. Commun.* **2016**, 7, 13638.
- 38. Mahmood, J.; Li, F.; Jung, S.-M.; Okyay, M. S.; Ahmad, I.; Kim, S.-J.; Park, N.; Jeong, H. Y.; Baek, J.-B. An efficient and pH-universal ruthenium-based catalyst for the hydrogen evolution reaction. *Nat. Nanotechnol.* **2017**, 12, 441-446.
- 39. Zhong, M.; Tran, K.; Min, Y.; Wang, C.; Wang, Z.; Dinh, C.-T.; De Luna, P.; Yu, Z.; Rasouli, A. S.; Brodersen, P.; Sun, S.; Voznyy, O.; Tan, C.-S.; Askerka, M.; Che, F.; Liu, M.; Seifitokaldani, A.; Pang, Y.; Lo, S.-C.; Ip, A.; Ulissi, Z.; Sargent, E. H. Accelerated discovery of CO₂ electrocatalysts using active machine learning. *Nature* **2020**, 581, 178-183.
- 40. Xu, H.; Rebollar, D.; He, H.; Chong, L.; Liu, Y.; Liu, C.; Sun, C.-J.; Li, T.; Muntean, J. V.; Winans, R. E.; Liu, D.-J.; Xu, T. Highly selective electrocatalytic CO₂ reduction to ethanol by metallic clusters dynamically formed from atomically dispersed copper. *Nat. Energy* **2020**, *5*, 623-632.
- 41. Jiang, K.; Sandberg, R. B.; Akey, A. J.; Liu, X.; Bell, D. C.; Nørskov, J. K.; Chan, K.; Wang, H. Metal ion cycling of Cu foil for selective C–C coupling in electrochemical CO₂ reduction. *Nat. Catal.* **2018**, 1, 111-119.
- 42. Chen, F.-Y.; Wu, Z.-Y.; Gupta, S.; Rivera, D. J.; Lambeets, S. V.; Pecaut, S.; Kim, J. Y. T.; Zhu, P.; Finfrock, Y. Z.; Meira, D. M.; King, G.; Gao, G.; Xu, W.; Cullen, D. A.; Zhou, H.; Han, Y.; Perea, D. E.; Muhich, C. L.; Wang, H. Efficient conversion of low-concentration nitrate sources into ammonia on a Ru-dispersed Cu nanowire electrocatalyst. *Nat. Nanotechnol.* **2022**, 17, 759-767.
- 43. Gao, Q.; Pillai, H. S.; Huang, Y.; Liu, S.; Mu, Q.; Han, X.; Yan, Z.; Zhou, H.; He, Q.; Xin, H.; Zhu, H. Breaking adsorption-energy scaling limitations of electrocatalytic nitrate reduction on intermetallic CuPd nanocubes by machine-learned insights. *Nat. Commun.* **2022**, 13, 2338.
- 44. Yan, Z.; Ji, M.; Xia, J.; Zhu, H. Recent Advanced Materials for Electrochemical and Photoelectrochemical Synthesis of Ammonia from Dinitrogen: One Step Closer to a Sustainable Energy Future. *Adv. Energy Mater.* **2020**, 10,

1902020.

- 45. An, S.; Liu, Z.; Bu, J.; Lin, J.; Yao, Y.; Yan, C.; Tian, W.; Zhang, J. Functional Aqueous Zinc–Acetylene Batteries for Electricity Generation and Electrochemical Acetylene Reduction to Ethylene. *Angew. Chem. Int. Ed.* **2022**, 61, e202116370.
- 46. Popczun, E. J.; McKone, J. R.; Read, C. G.; Biacchi, A. J.; Wiltrout, A. M.; Lewis, N. S.; Schaak, R. E. Nanostructured Nickel Phosphide as an Electrocatalyst for the Hydrogen Evolution Reaction. *J. Am. Chem. Soc.* **2013**, 135, 9267-9270.
- 47. Song, F.; Li, W.; Yang, J.; Han, G.; Liao, P.; Sun, Y. Interfacing nickel nitride and nickel boosts both electrocatalytic hydrogen evolution and oxidation reactions. *Nat. Commun.* **2018**, 9, 4531.
- 48. Mun, Y.; Lee, S.; Kim, K.; Kim, S.; Lee, S.; Han, J. W.; Lee, J. Versatile Strategy for Tuning ORR Activity of a Single Fe-N₄ Site by Controlling Electron-Withdrawing/Donating Properties of a Carbon Plane. *J. Am. Chem. Soc.* **2019**, 141, 6254-6262.
- 49. Liu, K.; Fu, J.; Lin, Y.; Luo, T.; Ni, G.; Li, H.; Lin, Z.; Liu, M. Insights into the activity of single-atom Fe-N-C catalysts for oxygen reduction reaction. *Nat. Commun.* **2022**, 13, 2075.
- 50. Yang, B.; Chen, L.; Xue, S.; Sun, H.; Feng, K.; Chen, Y.; Zhang, X.; Xiao, L.; Qin, Y.; Zhong, J.; Deng, Z.; Jiao, Y.; Peng, Y. Electrocatalytic CO2 reduction to alcohols by modulating the molecular geometry and Cu coordination in bicentric copper complexes. *Nat. Commun.* **2022**, 13, 5122.
- 51. Burke, L. D.; Lewis, F. A.; Kemball, C. Hydrogenation of acetylene at palladized palladium and platinized platinum electrodes. *Trans. Faraday Soc.* **1964**, 60, 919-929.
- 52. Davitt, H. J.; Albright, L. F. Electrochemical Hydrogenation of Ethylene, Acetylene, and Ethylene-Acetylene Mixtures. *J. Electrochem. Soc.* **1971**, 118, 236.
- 53. Bełtowska-Brzezinska, M.; Łuczak, T.; Mączka, M.; Baltruschat, H.; Müller, U. Ethyne oxidation and hydrogenation on porous Pt electrode in acidic solution. *J. Electroanal. Chem.* **2002**, 519, 101-110.
- 54. Otsuka, K.; Yagi, T. An Electrochemical Membrane Reactor for Selective Hydrogenation of Acetylene in Abundant Ethylene. *J. Catal.* **1994**, 145, 289-294.
- Huang, B.; Durante, C.; Isse, A. A.; Gennaro, A. Highly selective electrochemical hydrogenation of acetylene to ethylene at Ag and Cu cathodes. *Electrochem. Commun.* **2013**, 34, 90-93.
- 56. Yalkowsky, S.; He, Y.; Jain, P., *Handbook of Aqueous Solubility Data, Second Edition*. CRC Press: Boca Raton, FL, 2010.
- 57. Goyal, A.; Marcandalli, G.; Mints, V. A.; Koper, M. T. M. Competition between CO₂ Reduction and Hydrogen Evolution on a Gold Electrode under Well-Defined Mass Transport Conditions. *J. Am. Chem. Soc.* **2020**, 142, 4154-4161
- 58. Zhang, Z.; Chi, M.; Veith, G. M.; Zhang, P.; Lutterman, D. A.; Rosenthal, J.; Overbury, S. H.; Dai, S.; Zhu, H. Rational Design of Bi Nanoparticles for Efficient Electrochemical CO₂ Reduction: The Elucidation of Size and Surface Condition Effects. *ACS Catal.* **2016**, 6, 6255-6264.
- 59. Han, X.; Mou, T.; Liu, S.; Ji, M.; Gao, Q.; He, Q.; Xin, H.; Zhu, H. Heterostructured Bi–Cu2S nanocrystals for efficient CO₂ electroreduction to formate. *Nanoscale Horiz.* **2022**, 7, 508-514.
- 60. Park, S.; Lee, J.-W.; Popov, B. N. A review of gas diffusion layer in PEM fuel cells: Materials and designs. *Int. J. Hydrogen Energy* **2012**, 37, 5850-5865.
- 61. Ren, S.; Joulié, D.; Salvatore, D.; Torbensen, K.; Wang, M.; Robert, M.; Berlinguette, C. P. Molecular electrocatalysts can mediate fast, selective CO₂ reduction in a flow cell. *Science* **2019**, 365, 367-369.
- 62. Jeon, H. S.; Timoshenko, J.; Rettenmaier, C.; Herzog, A.; Yoon, A.; Chee, S. W.; Oener, S.; Hejral, U.; Haase, F. T.; Roldan Cuenya, B. Selectivity Control of Cu Nanocrystals in a Gas-Fed Flow Cell through CO₂ Pulsed Electroreduction. *J. Am. Chem. Soc.* **2021**, 143, 7578-7587.
- 63. Lin, R.; Guo, J.; Li, X.; Patel, P.; Seifitokaldani, A., Electrochemical Reactors for CO₂ Conversion. *Catalysts* **2020**, 10, 473.
- 64. Liang, S.; Altaf, N.; Huang, L.; Gao, Y.; Wang, Q. Electrolytic cell design for electrochemical CO₂ reduction. *J. CO2 Util.* **2020**, 35, 90-105.
- 65. Wan, L.; Xu, Z.; Xu, Q.; Wang, P.; Wang, B. Overall design of novel 3D-ordered MEA with drastically enhanced mass transport for alkaline electrolyzers. *Energy Environ. Sci.* **2022**, 15, 1882-1892.
- 66. Liu, Q.; Lan, F.; Chen, J.; Zeng, C.; Wang, J. A review of proton exchange membrane fuel cell water management: Membrane electrode assembly. *J. Power Sources* **2022**, 517, 230723.
- 67. Shi, R.; Wang, Z.; Zhao, Y.; Waterhouse, G. I. N.; Li, Z.; Zhang, B.; Sun, Z.; Xia, C.; Wang, H.; Zhang, T. Room-

- temperature electrochemical acetylene reduction to ethylene with high conversion and selectivity. *Nat. Catal.* **2021**, 4, 565-574.
- 68. Bai, R.; Li, J.; Lin, J.; Liu, Z.; Yan, C.; Zhang, L.; Zhang, J. Weak Acetylene Adsorption Terminated Carbon–Carbon Coupling Kinetics on Silver Electrocatalysts. *CCS Chemistry* **2022**, 5, 200-208.
- 69. Studt, F.; Abild-Pedersen, F.; Bligaard, T.; Sørensen Rasmus, Z.; Christensen Claus, H.; Nørskov Jens, K. Identification of Non-Precious Metal Alloy Catalysts for Selective Hydrogenation of Acetylene. *Science* **2008**, 320, 1320-1322.
- 70. Zhao, Z.-J.; Zhao, J.; Chang, X.; Zha, S.; Zeng, L.; Gong, J. Competition of C-C bond formation and C-H bond formation For acetylene hydrogenation on transition metals: A density functional theory study. *AIChE J.* **2019**, 65, 1059-1066.
- 71. Filhol, J.-S.; Neurock, M. Elucidation of the Electrochemical Activation of Water over Pd by First Principles. *Angew. Chem. Int. Ed.* **2006**, 45, 402-406.
- 72. Nørskov, J. K.; Rossmeisl, J.; Logadottir, A.; Lindqvist, L.; Kitchin, J. R.; Bligaard, T.; Jónsson, H. Origin of the Overpotential for Oxygen Reduction at a Fuel-Cell Cathode. *J. Phys. Chem. B* **2004**, 108, 17886-17892.
- 73. Taylor, C. D.; Wasileski, S. A.; Filhol, J.-S.; Neurock, M. First principles reaction modeling of the electrochemical interface: Consideration and calculation of a tunable surface potential from atomic and electronic structure. *Phys. Rev. B* **2006**, 73, 165402.
- 74. Chen, Z.; Cai, C.; Wang, T. Identification of Copper as an Ideal Catalyst for Electrochemical Alkyne Semi-hydrogenation. *J. Phys. Chem. C* **2022**, 126, 3037-3042.
- 75. Li, J.; Guo, Y.; Chang, S.; Lin, J.; Wang, Y.; Liu, Z.; Wu, Y.; Zhang, J. Pairing d-Band Center of Metal Sites with π-Orbital of Alkynes for Efficient Electrocatalytic Alkyne Semi-Hydrogenation. *Small* **2022**, 19, 2205845.
- 76. Bu, J.; Liu, Z.; Ma, W.; Zhang, L.; Wang, T.; Zhang, H.; Zhang, Q.; Feng, X.; Zhang, J. Selective electrocatalytic semihydrogenation of acetylene impurities for the production of polymer-grade ethylene. *Nat. Catal.* **2021**, 4, 557-564.
- 77. Grosse, P.; Yoon, A.; Rettenmaier, C.; Herzog, A.; Chee, S. W.; Roldan Cuenya, B. Dynamic transformation of cubic copper catalysts during CO₂ electroreduction and its impact on catalytic selectivity. *Nat. Commun.* **2021**, 12, 6736.
- 78. Lee, S. H.; Lin, J. C.; Farmand, M.; Landers, A. T.; Feaster, J. T.; Avilés Acosta, J. E.; Beeman, J. W.; Ye, Y.; Yano, J.; Mehta, A.; Davis, R. C.; Jaramillo, T. F.; Hahn, C.; Drisdell, W. S. Oxidation State and Surface Reconstruction of Cu under CO2 Reduction Conditions from In Situ X-ray Characterization. *J. Am. Chem. Soc.* **2020**, 143, 588–592.
- 79. Popović, S.; Smiljanić, M.; Jovanovič, P.; Vavra, J.; Buonsanti, R.; Hodnik, N. Stability and Degradation Mechanisms of Copper-Based Catalysts for Electrochemical CO2 Reduction. *Angew. Chem. Int. Ed.* **2020**, 59, 14736-14746.
- 80. Raaijman, S. J.; Arulmozhi, N.; Koper, M. T. M. Morphological Stability of Copper Surfaces under Reducing Conditions. *ACS Appl. Mater. Interfaces* **2021**, 13, 48730-48744.
- 81. Wang, S.; Uwakwe, K.; Yu, L.; Ye, J.; Zhu, Y.; Hu, J.; Chen, R.; Zhang, Z.; Zhou, Z.; Li, J.; Xie, Z.; Deng, D. Highly efficient ethylene production via electrocatalytic hydrogenation of acetylene under mild conditions. *Nat. Commun.* **2021**, 12, 7072.
- 82. Zhang, L.; Chen, Z.; Liu, Z.; Bu, J.; Ma, W.; Yan, C.; Bai, R.; Lin, J.; Zhang, Q.; Liu, J.; Wang, T.; Zhang, J. Efficient electrocatalytic acetylene semihydrogenation by electron–rich metal sites in N–heterocyclic carbene metal complexes. *Nat. Commun.* **2021**, 12, 6574.
- 83. Chang, S.; Bu, J.; Lin, J.; Lin, J.; Liu, Z.; Ma, W.; Zhang, J. Highly efficient electrocatalytic deuteration of acetylene to deuterated ethylene using deuterium oxide. *Chin. Chem. Lett.* **2022**, 107765.
- 84. Ma, W.; Chen, Z.; Bu, J.; Liu, Z.; Li, J.; Yan, C.; Cheng, L.; Zhang, L.; Zhang, H.; Zhang, J.; Wang, T.; Zhang, J. π-Adsorption promoted electrocatalytic acetylene semihydrogenation on single-atom Ni dispersed N-doped carbon. *J. Mater. Chem. A* **2022**, 10, 6122-6128.
- 85. Liu, Z.; Chen, Z.; Bu, J.; Ma, W.; Zhang, L.; Zhong, H.; Cheng, L.; Li, S.; Wang, T.; Zhang, J. Metal phthalocyanines as efficient electrocatalysts for acetylene semihydrogenation. *Chem. Eng. J.* **2022**, 431, 134129.
- 86. Resasco, J.; Abild-Pedersen, F.; Hahn, C.; Bao, Z.; Koper, M. T. M.; Jaramillo, T. F. Enhancing the connection between computation and experiments in electrocatalysis. *Nat. Catal.* **2022**, 5, 374-381.
- 87. Alfonso, D. R.; Tafen, D. N.; Kauffmann, D. R., First-Principles Modeling in Heterogeneous Electrocatalysis. *Catalysts*. **2018**, 8, 424.
- 88. Skúlason, E.; Tripkovic, V.; Björketun, M. E.; Gudmundsdóttir, S.; Karlberg, G.; Rossmeisl, J.; Bligaard, T.;

- Jónsson, H.; Nørskov, J. K. Modeling the Electrochemical Hydrogen Oxidation and Evolution Reactions on the Basis of Density Functional Theory Calculations. *J. Phys. Chem. C* **2010**, 114, 18182-18197.
- 89. Laursen, A. B.; Varela, A. S.; Dionigi, F.; Fanchiu, H.; Miller, C.; Trinhammer, O. L.; Rossmeisl, J.; Dahl, S. Electrochemical Hydrogen Evolution: Sabatier's Principle and the Volcano Plot. *J. Chem. Educ.* **2012**, 89, 1595-1599.
- 90. Skúlason, E.; Bligaard, T.; Gudmundsdóttir, S.; Studt, F.; Rossmeisl, J.; Abild-Pedersen, F.; Vegge, T.; Jónsson, H.; Nørskov, J. K. A theoretical evaluation of possible transition metal electro-catalysts for N₂ reduction. *Phys. Chem. Chem. Phys.* **2012**, 14, 1235-1245.
- 91. Montoya, J. H.; Tsai, C.; Vojvodic, A.; Nørskov, J. K. The Challenge of Electrochemical Ammonia Synthesis: A New Perspective on the Role of Nitrogen Scaling Relations. *ChemSusChem* **2015**, 8, 2180-2186.
- 92. Medford, A. J.; Vojvodic, A.; Hummelshøj, J. S.; Voss, J.; Abild-Pedersen, F.; Studt, F.; Bligaard, T.; Nilsson, A.; Nørskov, J. K. From the Sabatier principle to a predictive theory of transition-metal heterogeneous catalysis. *J. Catal.* **2015**, 328, 36-42.
- 93. Nørskov, J. K.; Abild-Pedersen, F.; Studt, F.; Bligaard, T. Density functional theory in surface chemistry and catalysis. *Proc. Natl. Acad. Sci. U. S. A.* **2011**, 108, 937-943.
- 94. Qiao, B.; Wang, A.; Yang, X.; Allard, L. F.; Jiang, Z.; Cui, Y.; Liu, J.; Li, J.; Zhang, T. Single-atom catalysis of CO oxidation using Pt1/FeOx. *Nature Chem.* **2011**, 3, 634-641.
- 95. Huang, F.; Deng, Y.; Chen, Y.; Cai, X.; Peng, M.; Jia, Z.; Ren, P.; Xiao, D.; Wen, X.; Wang, N.; Liu, H.; Ma, D. Atomically Dispersed Pd on Nanodiamond/Graphene Hybrid for Selective Hydrogenation of Acetylene. *J. Am. Chem. Soc.* **2018**, 140, 13142-13146.
- 96. Pei, G. X.; Liu, X. Y.; Yang, X.; Zhang, L.; Wang, A.; Li, L.; Wang, H.; Wang, X.; Zhang, T. Performance of Cu-Alloyed Pd Single-Atom Catalyst for Semihydrogenation of Acetylene under Simulated Front-End Conditions. *ACS Catal.* **2017**, 7, 1491-1500.
- 97. Shi, X.; Lin, Y.; Huang, L.; Sun, Z.; Yang, Y.; Zhou, X.; Vovk, E.; Liu, X.; Huang, X.; Sun, M.; Wei, S.; Lu, J. Copper Catalysts in Semihydrogenation of Acetylene: From Single Atoms to Nanoparticles. *ACS Catal.* **2020**, 10, 3495-3504.
- 98. Hibberd, G. E.; Parker, N. S. GAS PRESSURE VOLUME TIME RELATIONSHIPS IN FERMENTING DOUGHS .1. RATE OF PRODUCTION AND SOLUBILITY OF CARBON-DIOXIDE IN DOUGH. *Cereal Chem.* **1976**, 53, 338-346.
- 99. Zhang, M.; Wei, W.; Zhou, S.; Ma, D.-D.; Cao, A.; Wu, X.-T.; Zhu, Q.-L. Engineering a conductive network of atomically thin bismuthene with rich defects enables CO₂ reduction to formate with industry-compatible current densities and stability. *Energy Environ. Sci.* **2021**, 14, 4998-5008.
- 100. Ye, K.; Zhou, Z.; Shao, J.; Lin, L.; Gao, D.; Ta, N.; Si, R.; Wang, G.; Bao, X. In Situ Reconstruction of a Hierarchical Sn-Cu/SnOx Core/Shell Catalyst for High-Performance CO₂ Electroreduction. *Angew. Chem. Int. Ed.* **2020**, 59, 4814-4821.
- 101. Martindale, B. Go with the flow. *Nat. Catal.* **2020**, 3, 966-966.
- 102. Wheeler, D. G.; Mowbray, B. A. W.; Reyes, A.; Habibzadeh, F.; He, J.; Berlinguette, C. P. Quantification of water transport in a CO₂ electrolyzer. *Energy Environ. Sci.* **2020**, 13, 5126-5134.
- 103. Urmès, C.; Schweitzer, J.-M.; Cabiac, A.; Schuurman, Y. Kinetic Study of the Selective Hydrogenation of Acetylene over Supported Palladium under Tail-End Conditions. *Catalysts* **2019**, 9, 180.
- Lei, J.; Su, L.; Zeng, K.; Chen, T.; Qiu, R.; Zhou, Y.; Au, C.-T.; Yin, S.-F. Recent advances of catalytic processes on the transformation of alkynes into functional compounds. *Chem. Eng. Sci.* **2017**, 171, 404-425.
- 105. Oger, C.; Balas, L.; Durand, T.; Galano, J.-M. Are Alkyne Reductions Chemo-, Regio-, and Stereoselective Enough To Provide Pure (Z)-Olefins in Polyfunctionalized Bioactive Molecules? *Chem. Rev.* **2013**, 113, 1313-1350.
- 106. Fedorov, A.; Liu, H.-J.; Lo, H.-K.; Copéret, C. Silica-Supported Cu Nanoparticle Catalysts for Alkyne Semihydrogenation: Effect of Ligands on Rates and Selectivity. *J. Am. Chem. Soc.* **2016**, 138, 16502-16507.
- 107. Gao, Y.; Yang, R.; Wang, C.; Liu, C.; Wu, Y.; Li, H.; Zhang, B. Field-induced reagent concentration and sulfur adsorption enable efficient electrocatalytic semihydrogenation of alkynes. *Sci. Adv.* **2022**, 8, eabm9477.
- 108. Lee, M.-Y.; Kahl, C.; Kaeffer, N.; Leitner, W. Electrocatalytic Semihydrogenation of Alkynes with [Ni(bpy)₃]²⁺. *JACS Au* **2022**, 2, 573-578.
- 109. Li, H.; Gao, Y.; Wu, Y.; Liu, C.; Cheng, C.; Chen, F.; Shi, Y.; Zhang, B. σ-Alkynyl Adsorption Enables Electrocatalytic Semihydrogenation of Terminal Alkynes with Easy-Reducible/Passivated Groups over Amorphous PdSx Nanocapsules. *J. Am. Chem. Soc.* **2022**, 144, 19456-19465.
- 110. Liu, Z.; Zhang, L.; Ren, Z.; Zhang, J. Advances in Selective Electrocatalytic Hydrogenation of Alkynes to Alkenes. *Chem. Eur. J.* **2023**, 29, e202202979.
- 111. Ferrando, R.; Jellinek, J.; Johnston, R. L. Nanoalloys: From Theory to Applications of Alloy Clusters and

Nanoparticles. Chem. Rev. 2008, 108, 845-910.

- 112. Yan, Z.; Taylor, M. G.; Mascareno, A.; Mpourmpakis, G. Size-, Shape-, and Composition-Dependent Model for Metal Nanoparticle Stability Prediction. *Nano Lett.* **2018**, 18, 2696-2704.
- 113. Gao, Q.; Yao, B.; Pillai, H. S.; Zang, W.; Han, X.; Liu, Y.; Yu, S.-W.; Yan, Z.; Min, B.; Zhang, S.; Zhou, H.; Ma, L.; Xin, H.; He, Q.; Zhu, H. Synthesis of core/shell nanocrystals with ordered intermetallic single-atom alloy layers for nitrate electroreduction to ammonia. *Nat. Synth.* 2023, 2, DOI: 10.1038/s44160-023-00258-x.
- 114. Shen, J.; Kolb, M. J.; Göttle, A. J.; Koper, M. T. M. DFT Study on the Mechanism of the Electrochemical Reduction of CO2 Catalyzed by Cobalt Porphyrins. *J. Phys. Chem. C* **2016**, 120, 15714-15721.
- 115. Skúlason, E.; Karlberg, G. S.; Rossmeisl, J.; Bligaard, T.; Greeley, J.; Jónsson, H.; Nørskov, J. K. Density functional theory calculations for the hydrogen evolution reaction in an electrochemical double layer on the Pt(111) electrode. *Phys. Chem. Chem. Phys.* **2007**, 9, 3241-3250.